Final report

1.1 Project details

Project title	**Corrosion management in biomass firing**
Project identification (program abbrev. and file)	ForskEL - 2015-1-12289
Name of the programme which has funded the project	ForskEL
Project managing company/institution (name and address)	DTU Mechanical Engineering Niels Koppels Allé, bygning 404 2800 Kgs. Lyngby
Project partners	DTU Mechanical Engineering DONG Energy (Ørsted)
CVR (central business register)	30 06 09 46
Date for submission	09-09-2019

1.2 Short description of project objective and results

The project addressed corrosion in biomass fired power plants based on several years of collaboration between DTU and biomass fired heat and power plants in Denmark. The overall goal of the project was to develop and implement new tools for the management of corrosion problems in large-scale biomass firing based on improved understanding of corrosion mechanisms. This was obtained: a) In a ph.d project, which provided improved fundamental understanding of the influence of materials microstructure on the corrosion performance during long-term operation in biomass firing. And b) by collating and analyzing a large group of data from Danish biomass fired heat and power plants and developing quantitative models of corrosion rates as a function of material and corrosive environment.

Projektet omhandlede korrosion i biomassefyrede kraftvarmeværker med udgangspunkt i et mangeårigt samarbejde mellem DTU og biomassefyrede kraftvarmeværker i Danmark. Det overordnede projektmål var at udvikle og implementere nye værktøjer til håndtering af korrosion i storskala biomassefyring baseret på forbedret forståelse af mekanismerne for korrosion. Målet blev opfyldt ved: a) Gennemførelse af et ph.d. projekt, som tilvejebragte ny fundamental forståelse af indflydelsen af materialers mikrostruktur på deres korrosionsopførsel under landtids driftspåvirkning i biomasse fyring. Og b) ved at opsamle og analysere en stor mængde driftsdata fra danske biomassefyrede kraftvarmeværker og udvikle kvantitative modeller for korrosionshastigheder som funktion af materiale og korrosivt miljø.

1.3 Executive summary

Biomass contains highly aggressive species, which cause severe corrosion of the high temperature heat exchangers (superheaters) exposed to hot flue gases in boilers. Thus, high temperature corrosion is a major challenge for biomass-based heat and power production.

The present project addressed corrosion in biomass fired power plants based on several years of collaboration between DTU and biomass fired heat and power plants in Denmark. The overall goals of the project was

- To improve the fundamental understanding of the influence of materials microstructure on the corrosion performance during long-term operation in biomass firing
- To develop quantitative models of corrosion rates as a function of material and corrosive environment

The first goal of the project was realized in a ph.d. project, which unequivocally showed that precipitation of Cr rich phases such as Cr-carbides, sigma phase and alpha-Cr in steels an Ni base alloys leads to accelerating corrosion caused by direct corrosion attack of the precipitated phases.

This result reveals the previously unknown mechanism for internal corrosion in biomass firing and explains why steels with increasing Cr content higher than 18% shows more intense internal corrosion: They are simply more prone to formation of Cr rich phases.

Experience at grate fired Danish heat and power plants had shown the grates became brittle and lost weldability during long-term operation. Investigations in the project revealed that this was caused by nitridation of the grate surface due to the local chemistry at the surface.

To realize the second goal, a large set of investigation reports from previous collaboration between DTU and Danish biomass fired heat and power plants were collated into a database. Analysis of the data led to the formulation of a general model for corrosion in straw firing as a function of metal temperature.

The results of influence of materials microstructure on biomass corrosion are highly useful for the rebuilding of existing fossil fired plants to biomass firing, since it demonstrates that long-term operation resulting in a change of the materials microstructure leads to poorer corrosion performance. Further the results can be implemented to choose cheaper materials in future replacements of corroded parts in biomass fired plants.

The developed corrosion model is highly useful for the life assessment of superheaters and may lead to savings by avoiding loss unforeseen plant outages due to superheater corrosion as well as to optimum replacements of superheaters due to corrosion.

1.4 Project objectives

1.4.1. Background

Combustion of biomass in Danish decentralized CHP plants began in 1993, when the Danish government and utility operators made an agreement to use 1.4 mio. t. of biomass annually for power production in Denmark. This was implemented in small decentralized grate fired CHP plants firing straw or wood chips as well as by large scale use of biomass in central heat and power plants. Today, biomass combustion is a central element in the efforts to remove fossil fuels from the electricity production in Denmark.

Biomass contains highly aggressive species, which cause severe corrosion of the high temperature heat exchangers (superheaters) exposed to hot flue gases in boilers. Thus, high temperature corrosion is a major challenge for biomass based heat and power production.

Since the first use of biomass for heat and power production in 1993, a large number of in-situ tests of boiler materials have been carried out in Danish boilers in order to evaluate materials selection and corrosion rates as a function of steam temperature. The tests were carried out by utility companies in projects co-financed by EFP (Energi Forsknings Programmet) and PSO (ForskEL) and included both small grate fired boilers and co-firing of coal and biomass in large central power plants.

Systematic microstructure investigations of materials from the in-plant tests were conducted from 1997 at the Technical University of Denmark (DTU) in close collaboration with the major Danish utility companies. A gradually improved understanding of biomass corrosion was developed, which has been of great value in the handling of corrosion problems at biomass fired power plants.

The materials investigations at DTU concluded that austenitic steels with 18% Chromium and 10% Nickel offered the best corrosion resistance among existing superheater tube materials. Further, it was found that steam temperatures higher than 540ºC lead to strongly accelerated corrosion rates. Surprisingly, materials with higher Cr content - which show better corrosion resistance in many other corrosive environments - showed accelerating corrosion in biomass firing. The reason for this behavior was not well understood.

1.4.2. Project goals

The overall goal of the project was to develop and implement new tools for the management of corrosion problems in large-scale biomass firing based on improved understanding of corrosion mechanisms. This is obtained via two sub goals:

- To improve the fundamental understanding of the influence of materials microstructure on the corrosion performance during long-term operation in biomass firing
- To develop quantitative models of corrosion rates as a function of material and corrosive environment

It was an additional goal of the project to maintain the strong research environment at DTU Mechanical Engineering in a transition period, where new operators become active in the production of heat and power from biomass combustion.

1.4.3. Project content and milestones

It is hypothesized that phase transformations in superheater steels significantly affect their corrosion performance. This can explain why steels with more than 18% Cr show accelerating corrosion, and could also affect the long-term behavior of the favored 18%Cr steels. This hypothesis was investigated by dedicated laboratory experiments at DTU and results were validated by in-depth microstructure investigations of selected (long-term) exposed materials removed from power plants (Milestone 1).

Thermodynamic and kinetic modeling of the phase transformations are combined with empirical or semi-empirical models of corrosion to enable predictions of corrosion rates as a function of material, environment and temperature profiles (Milestone 2).

Sample removals made from running power plants in order to monitor corrosion as a function of fuel, plant type, exposure temperatures and material type. Other effects like e.g. fuel switching (memory effects) could also be evaluated. (Milestone 3).

Microstructure investigations of removed materials are made at DTU in order to build up a database of corrosion rates, which provide input to the development of corrosion models. Materials investigations are made from selected historical cases involving e.g. plant failures or exposures of special materials. The database include results from previous investigations (Milestone 4).

The project is coordinated by DTU. Project meetings are held to present results to project partners and facilitate information exchange and discussions between university researchers and plant operators (Milestone 5).

1.4.3 Project implementation

The project was defined by DTU Mechanical Engineering and carried out in collaboration with DONG Energy. The project was implemented in three work packages:

WP1 Corrosion and steel microstructure included research in a Ph.D. project at DTU Mechanical Engineering to improve the fundamental understanding of the influence of materials microstructure on corrosion. Kinetic models of the influence of microstructure evolution are developed.

WP2 Corrosion database and models included microstructure investigations at DTU Mechanical Engineering of removed samples from power plants. Sample removals were planned in collaboration with DONG Energy, who delivered samples to DTU. Materials from earlier plant removals for in-depth microstructure investigations were available at DTU. Results were organized in a database and used to develop empirical or semi-empirical models of corrosion.

WP3 Project coordination included project meetings and dissemination activities.

The project was initiated on March 1, 2015 and finalized on June 30, 2019, which was a delay of 11 months according to the original plan.

The research part of the project was carried out by staff at DTU Mechanical Engineering. Senior researcher Melanie Montgomery was employed from March 1, 2015 and left DTU on May 31, 2019. She carried out the main activities in WP2. Ph.D. student Yohanes Chekol Malede was employed at DTU in the period March 1, 2016 to February 28, 2019. Yohanes Malede stood out as the best qualified amongst the 40+ applicants for the publicly advertised Ph.D. project, so it was decided to wait for him to finish his final M.Sc. exams. This was the sole cause for the delay of the project according to the original plan.

Yohanes Malede carried out his ph.d. project without delays. He successfully defended his ph.d. thesis on May 14, 2019.

Risks in the project were related to the loss of the research environment at DTU in a period where the ownership of biomass fired plants changed from large regional companies (DONG Energy and Vattenfall) to smaller localized companies. This risk was handled by holding a series of user group meetings with the major owners of CHP plants in Denmark. New research has been initiated to continue the activities at DTU after the end of the project.

Other risks were associated with the success of the research work. Obtained results are described below.

1.5 Project results and dissemination of results

Project results are presented in the three work packages

1.5.1 WP1 – Corrosion and steel microstructures

1.5.1.1 Background for Ph.D project

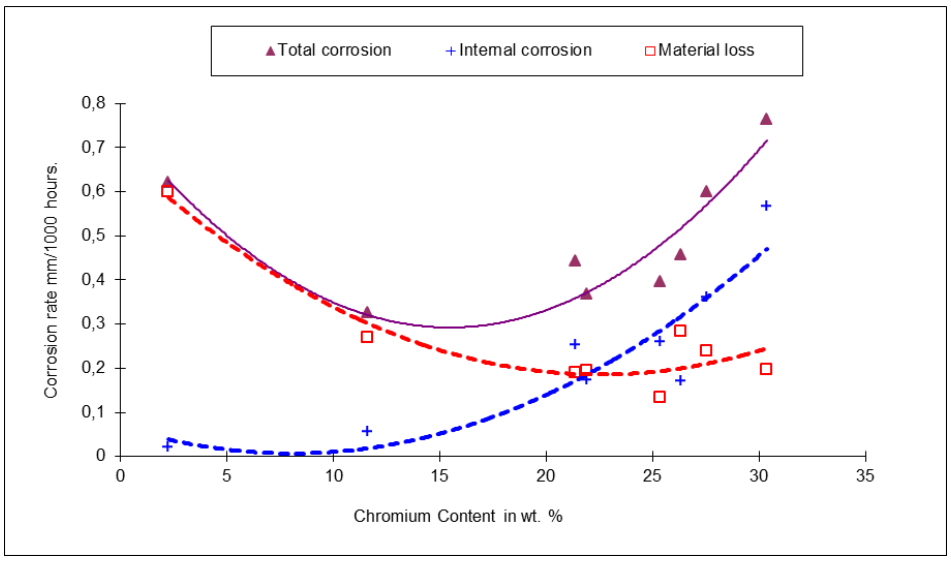

Figure 1: Corrosion rates for different materials exposed on a cooled probe.

Corrosion testing had been undertaken with a cooled corrosion probe inserted in the boiler of a straw-firing plant above the combustion zone [1]. The exposure time was 1392 hours where the probe temperature fluctuated around 450-580^{0}C. Thus corrosion rates with respect to a specific temperature could not be given; however a ranking of materials with the fluctuating temperature and operating conditions was obtained. The specimens were measured for corrosion attack, where the materials loss was based on initial pre-exposure thickness measurements. The results from this test revealed that corrosion attack (▲) could be divided into two components, material loss (□) and internal attack (+) as shown in Figure 1. Lower material loss was observed for chromium rich alloys; however these alloys suffered from increased internal attack. The alloys with high iron content revealed very little internal attack, whilst alloys with higher chromium content were internally attacked at i) grain boundaries or ii) within the grain resulting in a porous structure or iii) both.

The 2.25%Cr ferritic steel suffered from minimal internal corrosion, and the amount of internal corrosion was slightly deeper for the 12% Cr steel. In contrast, the alloy with highest chromium content experienced material loss similar to the other steels (apart from the lowest alloyed steel) but instead had the highest depth of internal attack together with chromium depletion.

Thermodynamics calculations can be used to evaluate whether alloys have a tendency towards forming chromium rich precipitates that may be preferentially attacked 5. This can also help to gain an understanding of the mechanisms behind the accelerated internal corrosion observed in high Cr containing materials. Thermodynamics calculations revealing phase precipitation of the steel and alloy types investigated in Figure 2 are given in Table 1. It is revealed that the materials which incurred high internal attack coincide with those where the precipitation of Cr-rich phases such as alpha chromium (α-Cr) and sigma phase (σ-phase) are calculated. Unfortunately the samples were no longer available for further microstructure analysis, but the materials predicted to form the very Cr rich (>90wt% Cr) alpha chromium are the ones with the highest tendency towards internal corrosion as shown in Figure 2. Sigma phase is also Cr-rich but typically only forms after long exposure times and therefore would not influence short exposures.

Table 1: Thermodynamical calculations performed in Thermo-Calc revealing phase precipitation at the average exposure temperature of the alloys, 550˚C [5].

	Cr wt%	Cr at%	Selective corrosion rate mm/1000h	FCC	ALFA-Cr	SIGMA	P_PHASE	NBNI3	NI3TI	M23C6	TiC
Alloy B	30.3	32.5	0.58	0.802	0.188	-	0.004	-	-	0.006	-
Sanicro 28	27.5	29.7	0.37	0.675	0.082	0.238	-	-	-	0.004	-
Sanicro 38	21.3	22.8	0.26	0.808	0.064	0.098	-	-	0.026	-	0.003
Sandvik 8RE 10	25.4	26.9	0.26	0.770	-	0.093	-	-	-	0.137	-
Sanicro 63	21.9	24.9	0.18	0.695	-	-	0.199	0.080	0.004	0.022	-
Alloy A	26.3	27.9	0.18	0.616	-	0.352	-	0.013	-	0.020	-
X20CrMoV121	11.6		0.05								
10CrMo910	2.2		0.02								

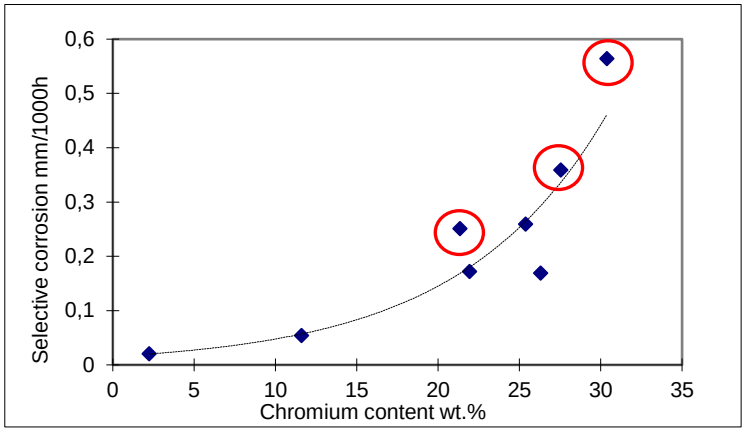

Figure 2: Internal attack of alloys shown in Figure 1, where the alloys with stable alpha precipitation are marked 5.

Based on these observations the internal corrosion and precipitation during ageing was investigated in the Ph.D. project.

1.5.1.2 Objectives of the Ph.D. project

Up until now it had been assumed that the corrosion rate of as received materials is similar to that of exposed specimens, however this could be an over simplification. With ageing, precipitation reactions occur that can influence the corrosion behavior by promoting internal attack. Based on the reviewed literature, the following mechanisms were speculated as possible reasons for the selective internal attack of high Cr alloys:

- The precipitation of Cr rich phases (σ-phase, Cr rich carbides etc.) and the interaction of these phases with Cl species to form high volatile chromium chloride.
- Grain boundaries as pathways for ingress of Cl resulting in selective attack of Cr to form chromium chloride.
- Sensitisation due to the precipitation of Cr rich phases.
- In some cases, melts can be formed from eutectic mixtures of metal chlorides with KCl, or directly from low melting chlorides, in that case galvanic coupling between the Cr rich phase and the matrix could play a role in selective attack.

Hence, understanding the effect of microstructure (with an emphasis on Cr-rich phases) on biomass-induced corrosion was the key element of the Ph.D. study.

The research activities in the Ph.D. project involved laboratory experiments, materials characterisation including advanced electron microscopy characterisation, as well as computer modelling to simulate results obtained from the experimental work. The focus of the study was to understand the mechanisms of selective internal corrosion which is the propagation reaction observed in high Cr steels in biomass fired power plants. Previous research had focused on the initiation reactions with respect to breakdown of protective oxides [2], varying corrosive gas compositions with and without KCl [3], and development of protective coatings [4]. Investigations regarding internal attack of high temperature materials were few in number and microstructures before and after exposures were generally not well characterized.

Coupling the microstructural change with KCl-induced corrosion is important in the design and the lifetime prediction of superheaters and similar components. In the boiler there are variable conditions such as changes in fuel, temperature, heat flux, thermal cycling, however in the laboratory a fixed exposure was chosen to reveal how precipitation affects KCl corrosion. The exposures were undertaken at 600°C for 168 hours in flowing gas (15%H_2O+ 5%O_2+ N_2) with and without the presence of a KCl deposit. Materials that give widely different microstructures due to thermal ageing were specifically selected for corrosion exposures (compositions given in Table 2). In addition, to exclude effects related to precipitation of Cr rich phases within a matrix or on a grain boundary (such as sensitisation and galvanic corrosion etc.) direct corrosion responses of Cr-rich phases were investigated by producing surface layer coatings of only Cr-rich carbide and Cr rich σ-phase. Table 3 shows the materials investigated and the amount of precipitates they contained.

Table 2: Compositions of the studied materials.

Wt. %	Cr	Ni	Cu	Mn	W	C	Si	Nb	V	Ti	N	O	Fe
Modified AISI 310	22.3	22	2.77	0.84	2.46	0.088	0.023	0.36	0.36	0.27	0.03	-	Bal.
AISI 347H FG	19.7	12.5	-	1.5	-	*	0.7	0.5	-	-	-	-	Bal.
Ni35Cr4Nb	34.4	Bal.	-	-	-	0.011	0.03	3.8	-	0.5	0.002	0.03	0.03
Ni45Cr4Nb	44.8	Bal.	-	-	-	0.013	0.05	4.1	-	0.5	0.002	0.03	0.03
AISI O1	0.5	-	-	1.2	0.5	0.9	0.3	-	0.3	-	-	-	Bal.

Table 3: Microstructures of the studied materials (in terms of Cr-rich phases).

Material	Condition	Microstructure (fraction of Cr-rich precipitate)
Modified 310	As-received / solution treated	0 % σ-phase per area
	Aged (700 °C, 10 000 h)	29 % σ-phase per area
AISI 347H FG	As-received / acid pickled condition	0 % σ-phase per area
	A 'real' reheater material service exposed in a coal fired power plant for 100 000 h	Up to 8 % σ-phase per area
Ni35Cr4Nb	Solution treated	≈ 0 % α-Cr per area
	Aged (650 °C for 6000 h)	12 % α-Cr per area
Ni45Cr4Nb	Solution treated	19 % α-Cr per area
	Aged (650 °C for 6000 h)	26 % α-Cr per area
Substrates	layer	
AISI 01 steel	Cr-rich carbide layers	
AISI 347H FG and Modified AISI 310	Cr-rich σ-phase layers	

For all the materials exposed in KCl atmosphere, the formation of K_2CrO_4 was observed at the surface as shown by others e.g. [6,7] indicating that Cr_2O_3 cannot form a protective oxide in the presence of KCl. This reaction occurred regardless of the microstructure of the underlying alloy (Figure 3), i.e. both on aged and as received (solution treated) alloys. Thus the initiation reaction was similar on all tested alloys.

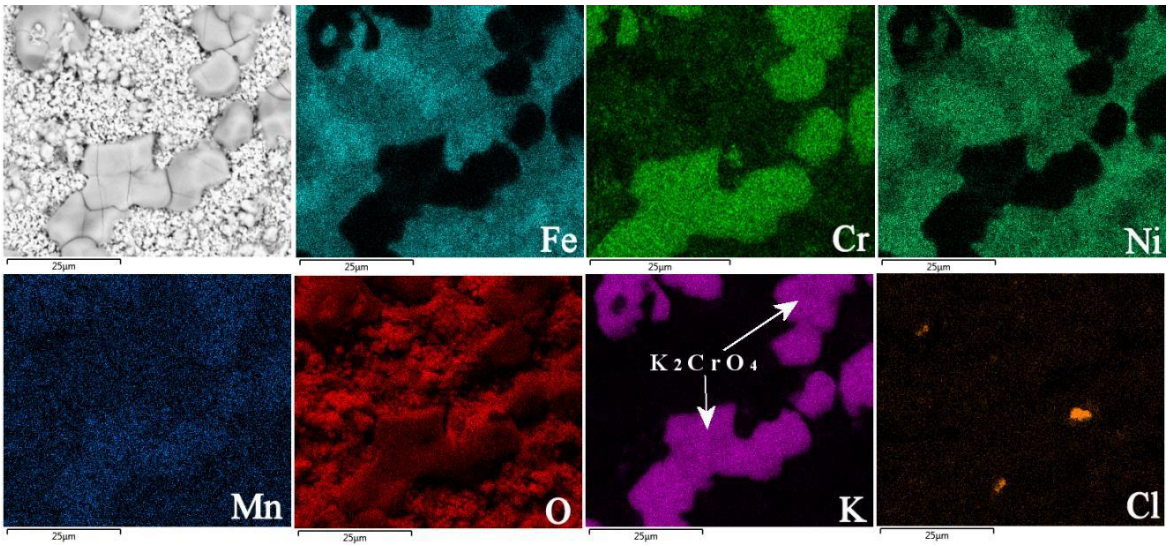

Figure 3: BSE micrograph and elemental maps (surface-view) of KCl-covered chromized modified AISI 310 steel exposed to a 15 % (v/v) H_2O (g) + 5 % (v/v) O_2 (g) + N_2 (g) (balance) atmosphere at 600 °C for 168 h.

In addition thermodynamics and kinetics modelling was undertaken with Thermocalc and DICTRA programs to predict precipitation reactions, growth of precipitates and which parameters were important, and also reactions between the alloy and KCl in an oxidising environment.

1.5.1.3 Effects of σ-phase and α-Cr phase on KCl-induced corrosion

A modified AISI 310 steel was chosen to investigate the influence of σ-phase (a Cr-rich intermetallic phase) on KCl-induced corrosion. The modified AISI 310 steel was a targeted choice that would allow testing of the same material with two widely different microstructures (Figure 4). Corrosion experiments were carried out using the modified AISI 310 steel in the as-received (solution treated) condition (no substantial amount of σ-phase) and heat-treated condition (29 % of σ-phase per area). To evaluate the interaction of σ-phase with KCl, corrosion exposures were done using KCl-free (reference) and KCl-covered samples in the laboratory environment previously mentioned.

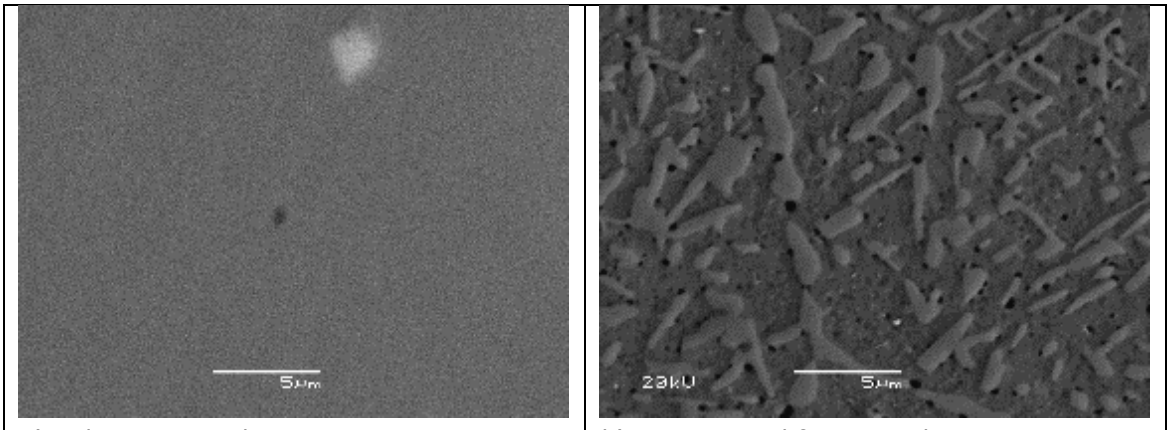

a) Solution treated | *b) Heat treated for 10000 hours at 700°C*

Figure 4: Comparison of microstructures for modified 310 steel.

This specific steel was chosen since heat treatment at 700°C for 10000 hours results in sigma phase but if the steel is heat treated at 650°C, sigma phase does not precipitate. However it was of interest to use an extreme case to see if after 168h at 600°C, there was a measurable difference in attack between the two microstructures.

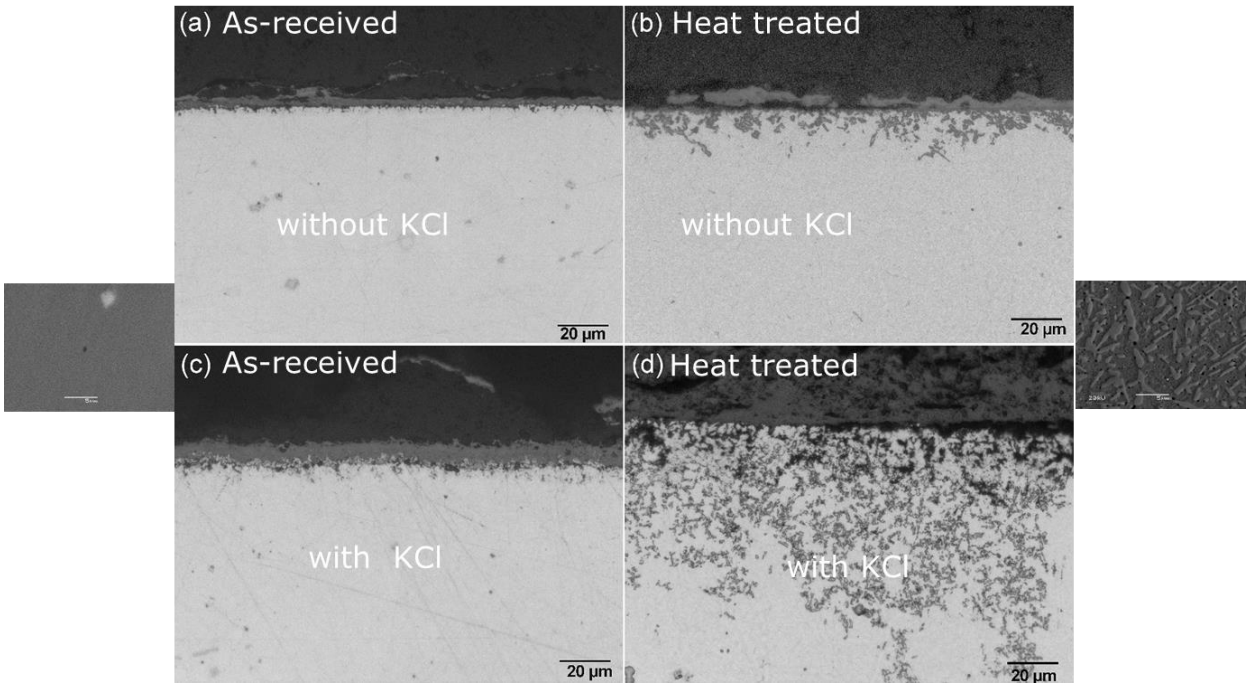

Figure 5: Comparison of corrosion response for the same steel where the heat treated steel had formed Cr rich sigma phase.

It was found that σ-phase had a detrimental effect when KCl was present compared to the reference condition without KCl. The presence of σ-phase in the heat-treated material drastically increased the KCl induced corrosion attack of the heat-treated material: the heat-treated material (that had 29 % of σ-phase) showed a fivefold sound metal loss compared to the as-received material (that had no σ-phase) and the phase that was preferentially attacked was sigma phase [8].

From TEM analysis adjacent the sigma phase before exposure, no composition gradient was observed, however after exposure Cr depletion at the corrosion front was measured (Figure 6).

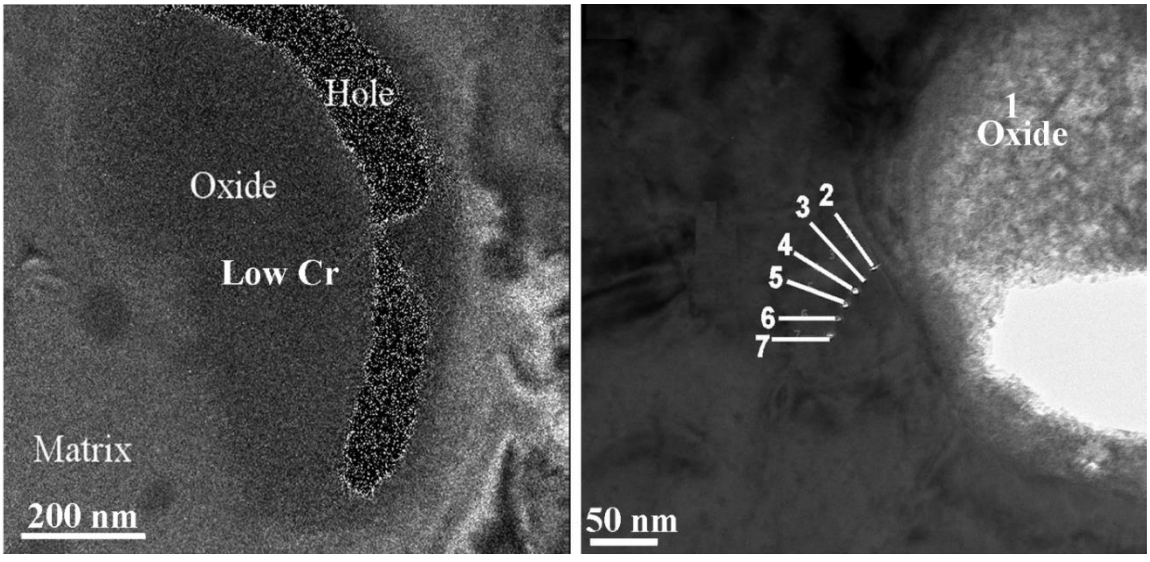

Wt. %	O	Mn	Cl	Cr	Fe	Ni	W
1 Oxide	24.2	-	4.4	6.5	16.7	33.1	15.1
2	-	0.76	-	15.8	54.0	29.4	-
3	-	-	-	17.8	55.1	27.1	-
4	-	-	-	18.8	54.8	27.1	-
5	-	-	-	19.4	54.2	26.3	-
6	-	-	-	19.9	53.6	26.4	-
7	-	-	-	20.2	53.2	26.6	-

Figure 6: TEM analysis of KCl corroded area at the corrosion front. Cr depletion adjacent the corrosion front.

Inspired by these findings, it was relevant to assess the corrosion response of actual high temperature heat exchanger materials. A sample was taken from the middle of the tube of a service exposed reheater fabricated from TP347H FG. The reheater tube had been exposed to a steam temperature of 535°C and a flue gas, which had a temperature of 1100 ^{o}C for approximately 100000h at Nordjyllandsværket, and the tube had estimated metal temperatures of 585 ^{o}C and 570 ^{o}C in the flue gas and opposite to the flue gas directions respectively. From microstructure assessment, sigma phase had been identified in the bulk of the tube thickness to varying extents (more where the metal temperature was estimated to be slightly higher) but was not present in the as received steel (Figure 7). The corrosion response of the service exposed and as received steels was compared in the laboratory KCl containing environment. This is a very relevant comparison since retrofitting of coal fired boilers occurs, and the comparison of corrosion rates from as received steel and aged steel is important, as it would be the aged steel that is more relevant for lifetime prediction of these boilers.

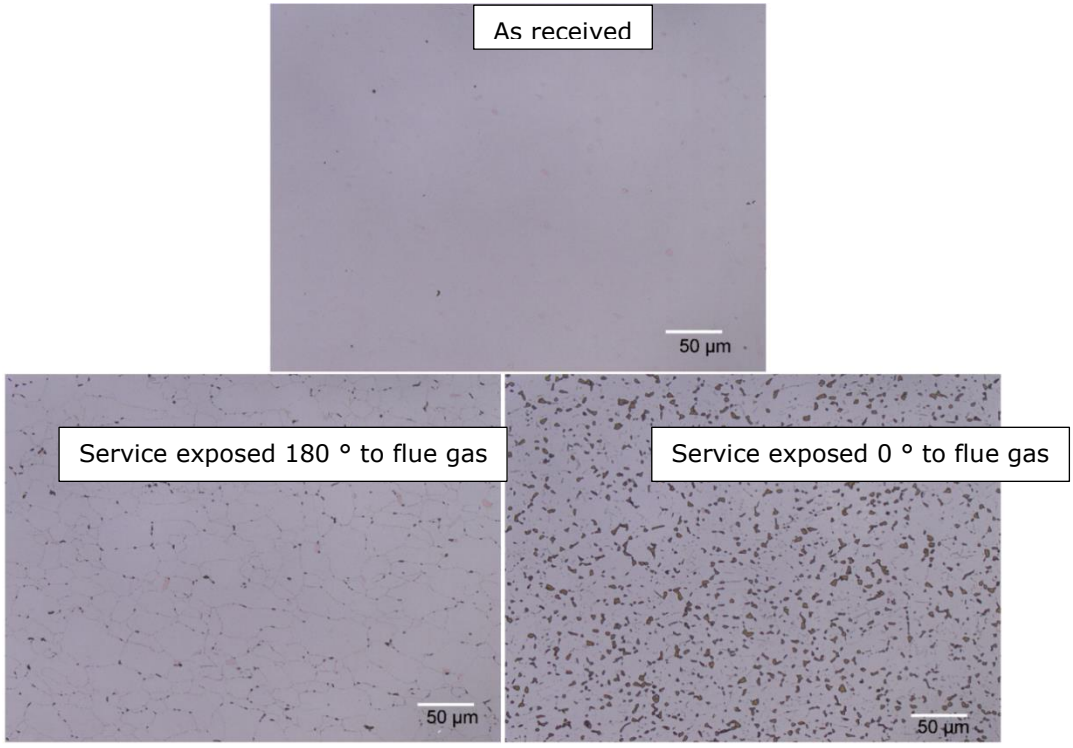

Figure 7: Comparison of etching response on as received and service exposed 347H FG after etching with KOH.

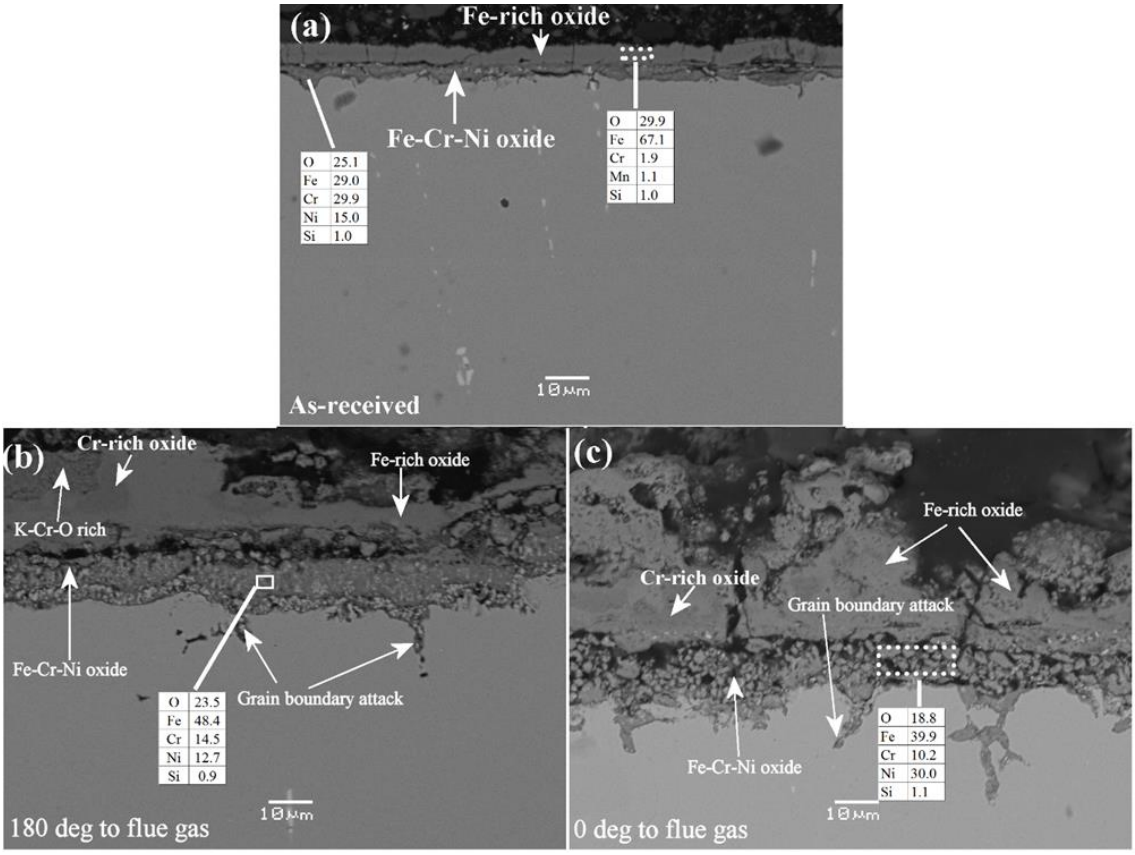

Figure 8: Comparison of attack on as received and service exposed 347H FG.

From this it was clear that there was more attack on the aged bulk microstructure (Figure 8), however it could not be concluded that the microstructure with more sigma phase had more corrosion. Thus service exposure resulting in σ phase formation has an adverse effect on KCl induced high temperature corrosion of AISI 347H FG. It was observed that the corrosion attack in the service exposed material was propagated at an accelerated rate by a selective chlorine attack of Cr-rich σ-phase.

1.5.1.4 Effects of α-Cr phase on KCl-induced corrosion

As discussed in the introduction, reassessment of previous data had indicated that higher corrosion rates from different metals exposed in a straw-firing plant could be due to the formation of α-Cr (Cr-rich phase), similar to that observed with σ-phase. Thus similar experiments were undertaken to investigate KCl attack on α-Cr, and also if the amount of α-Cr could be related to the depth of attack. For this investigation, two Ni-Cr alloys were chosen and subjected to heat treatments which resulted in various amounts of α-Cr being formed, such that the relative amounts of α-Cr as a parameter could be tested. This was of interest as it was clear with the service exposed bulk material, that the degree of attack was similar although the amount of sigma phase was different. For this purpose, Ni-(35-45) Cr-4Nb alloys containing (~0, 12.4 ±1.0, 19.2±1.1, 26.1±1.5) vol. % of α-Cr were investigated (Figure 9).

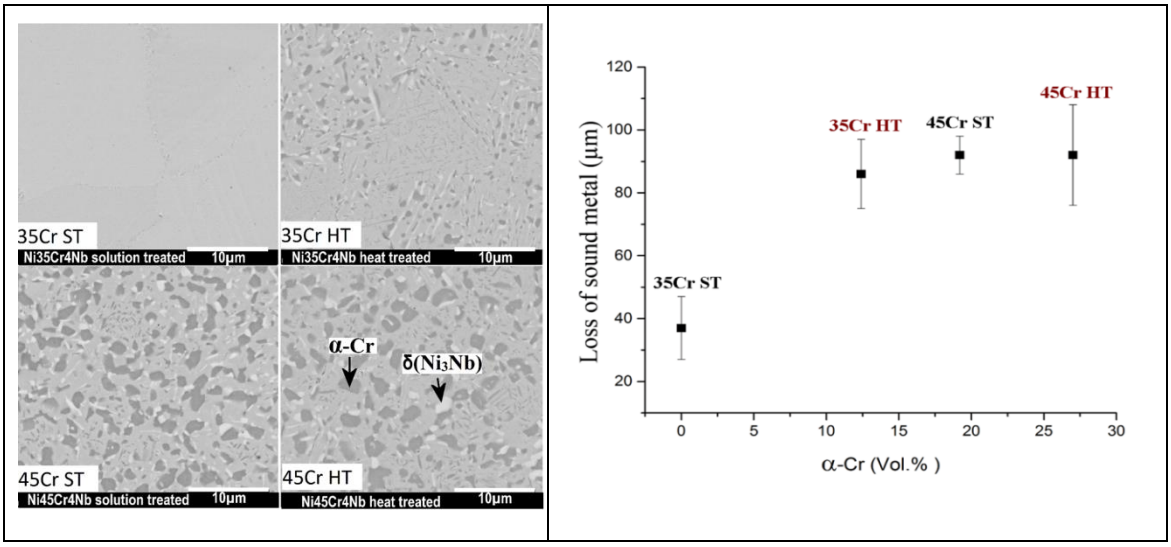

Figure 9: Microstructure of Ni alloy with varying amounts of α-Cr and corrosion depth with respect to vol.% of α-Cr

It was clear that the presence of α-Cr led to accelerated corrosion in KCl bearing environments. However, increasing volume fractions of α-Cr (from 0.12 to 0.26) did not result in increased attack. Where there was no α-Cr, there was a thin layered corrosion product, and there was both internal attack and phase dissolution of the α-Cr (Figure 10). The attack could be linked to the size of the precipitates. In addition to Cr rich precipitates being attacked, it was also clear that Nb rich precipitates were also attacked but to a lesser extent. The reason for the attack of Cr and Nb precipitates can be explained by thermodynamic modelling [9].

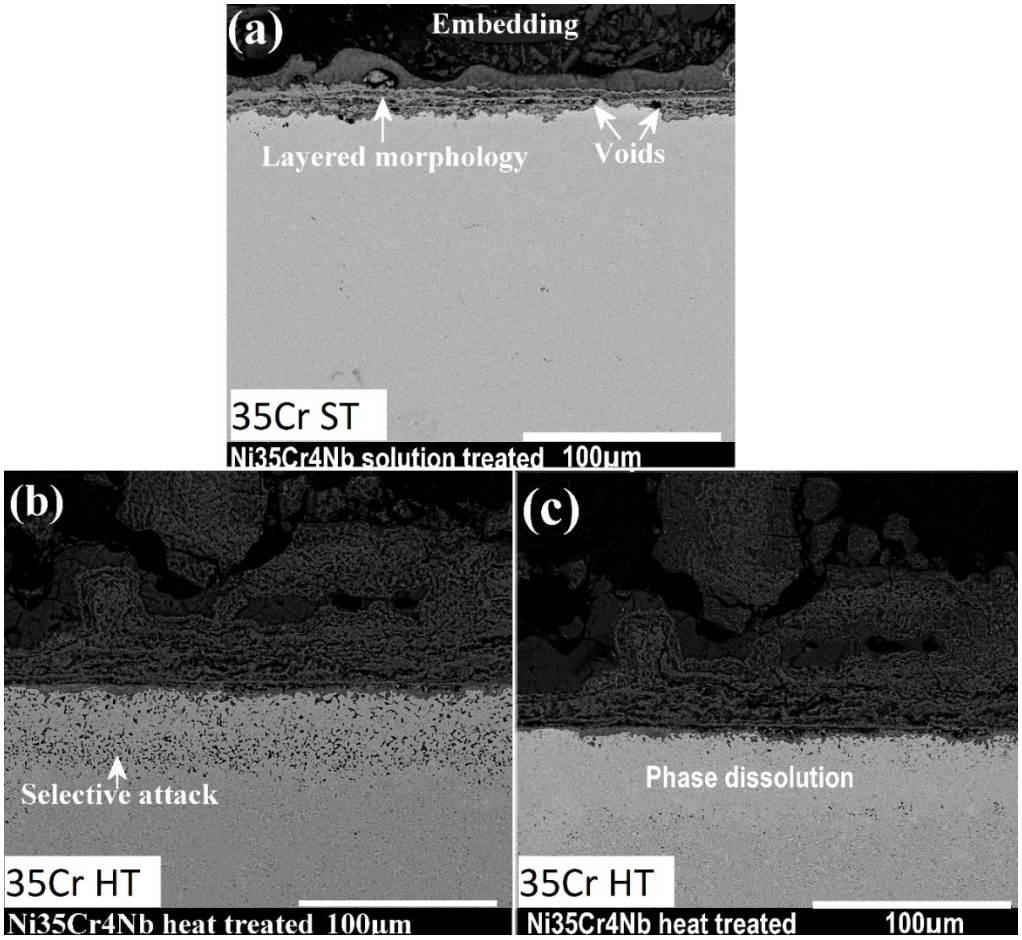

Figure 10: Morphology of attack of heat treated and solution treated Ni35%Cr alloys.

1.5.1.5 Corrosion behaviour of Cr-rich surface layers

Cr depleted interfaces around Cr precipitates can play their own role in the observed accelerated corrosion of Cr-rich precipitate containing materials. To reduce limitations related to investigating Cr-rich precipitates within a matrix (such as sensitization and galvanic corrosion), and to investigate the direct interaction of KCl with the Cr-rich phases, corrosion exposures were done using continuous surface layers of σ-phase and Cr-rich carbides. Corrosion experiments were conducted as previously mentioned. The KCl-free samples showed remarkable oxidation resistance, but Cr-rich phases were totally attacked in the KCl-covered samples. Figure 11a shows the original coating which consisted of various chromium carbides (Cr=M), the coating after exposure in the gaseous oxidizing environment (Figure 11b and the surface of the sample after exposure in the KCl bearing environment (Figure 11c). In the latter, there were low levels (<5 wt.%) of Cr detected within the outer 5μm of the total 58μm oxide.

Other experiments where a surface layer of σ-phase has been tested, a complete removal of the Cr rich σ-phase was also observed. This reveals that it is the precipitates themselves that react with the KCl, and matrix effects are secondary.

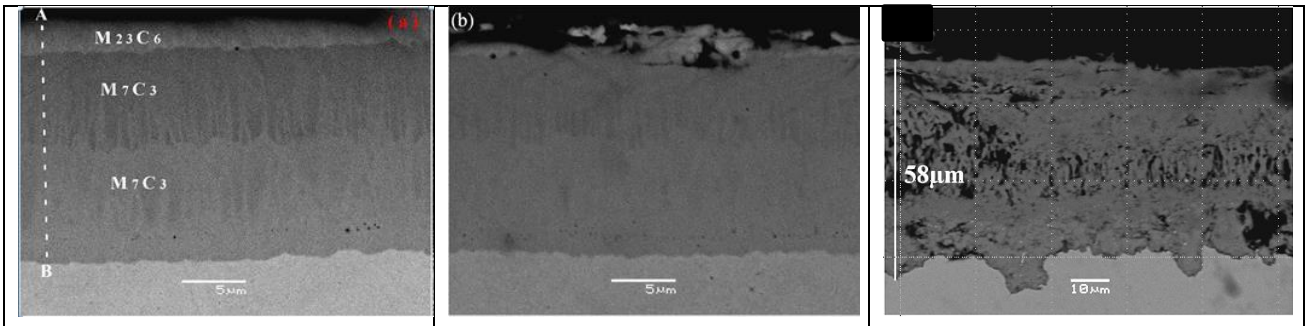

a) Cr carbide surface layers	*b) exposure to gas environment*	*c) Exposure to the gas environment +KCl*

Figure 11: Micrographs of pre-exposure and post exposure results with Cr carbide layers

1.5.1.6 Modelling with thermodynamic and diffusion databases

Thermodynamic modelling databases (ThermoCalc and Matcalc) were used to predict the phases present when a system has reached equilibrium at a defined temperature [10]. Employing such prediction tools will give an indication with respect to whether precipitates which are susceptible to attack will be in equilibrium at the temperatures concerned. Whether they are actually present will depend on the nucleation and growth of the precipitates. An example of this for the Ni-Cr alloys shows the relative amounts of α-Cr and δ(Ni_3Nb) predicted for the solution treated alloy and the heat treated alloy. The predictions shown in Figure 12 were in general agreement with microstructure observations in Figure 9.

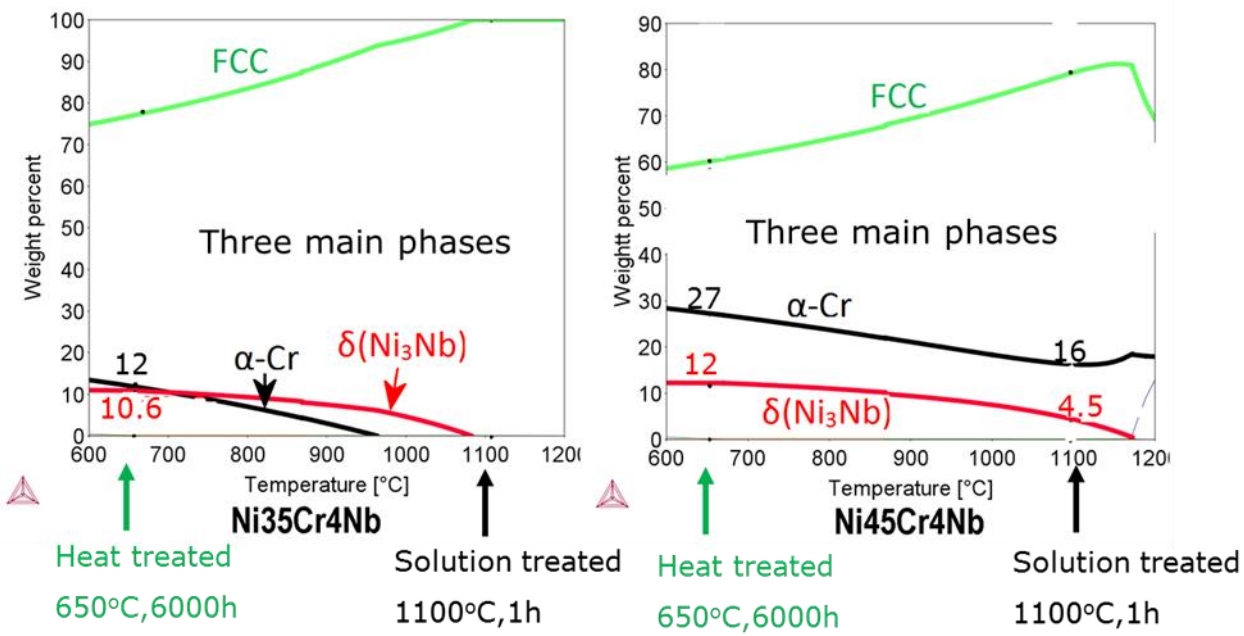

Figure 12: Phases predicted for the Ni-Cr alloys pre and post heat treatment.

Calculations were also undertaken to understand the preferential attack observed for the specific sigma phase formed for the 347H steel. Figure 13 shows the stability of Cr rich sigma phase which has a lower stability than austenite in chlorine bearing environments.

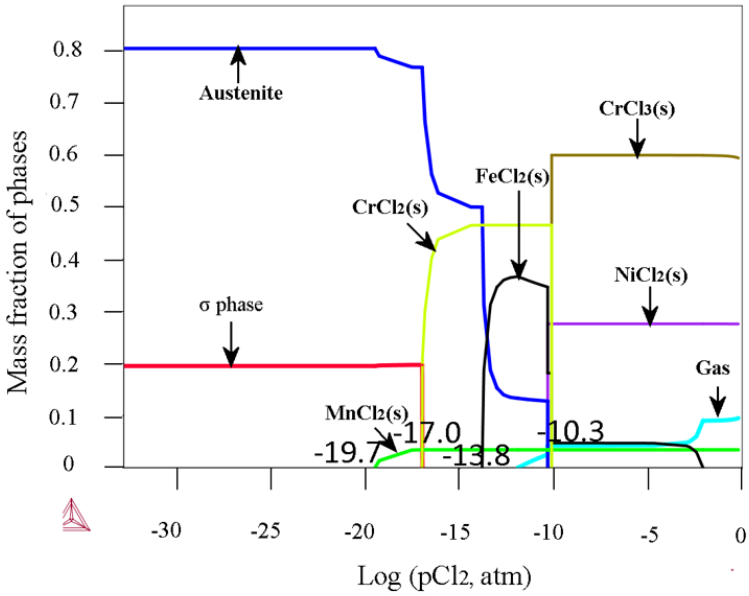

Figure 13: Stability diagram of austenite and sigma phase in 347H steel.

The adverse effect of Cr-rich phases on high temperature KCl induced corrosion has been clearly shown in the previous sections. Hence, it is intriguing to study the growth kinetics of Cr-rich phases in alloys due to thermal ageing. The growth kinetics of σ-phase in austenite matrix of AISI 347H FG steel was simulated using DICTRA with grain boundary assisted diffusion [11]. The focus of the simulation work was to calculate the size evolution (radius and volume fraction) of σ-phase as a function of time and temperature. Plotting the concentration profile of the alloying elements around σ-phase was also part of the objective. Simulations using

DICTRA predicted Cr-depletion zones around σ-phase in the service exposed AISI 347H FG steel which were confirmed experimentally with STEM investigations. The study also included the effects of temperature, composition of alloying elements, grain size, and grain boundary thickness on the growth kinetics of σ-phase. This is important if the difference between a fine and a coarse-grained steel are compared, or the difference that may occur with allowable steel composition.

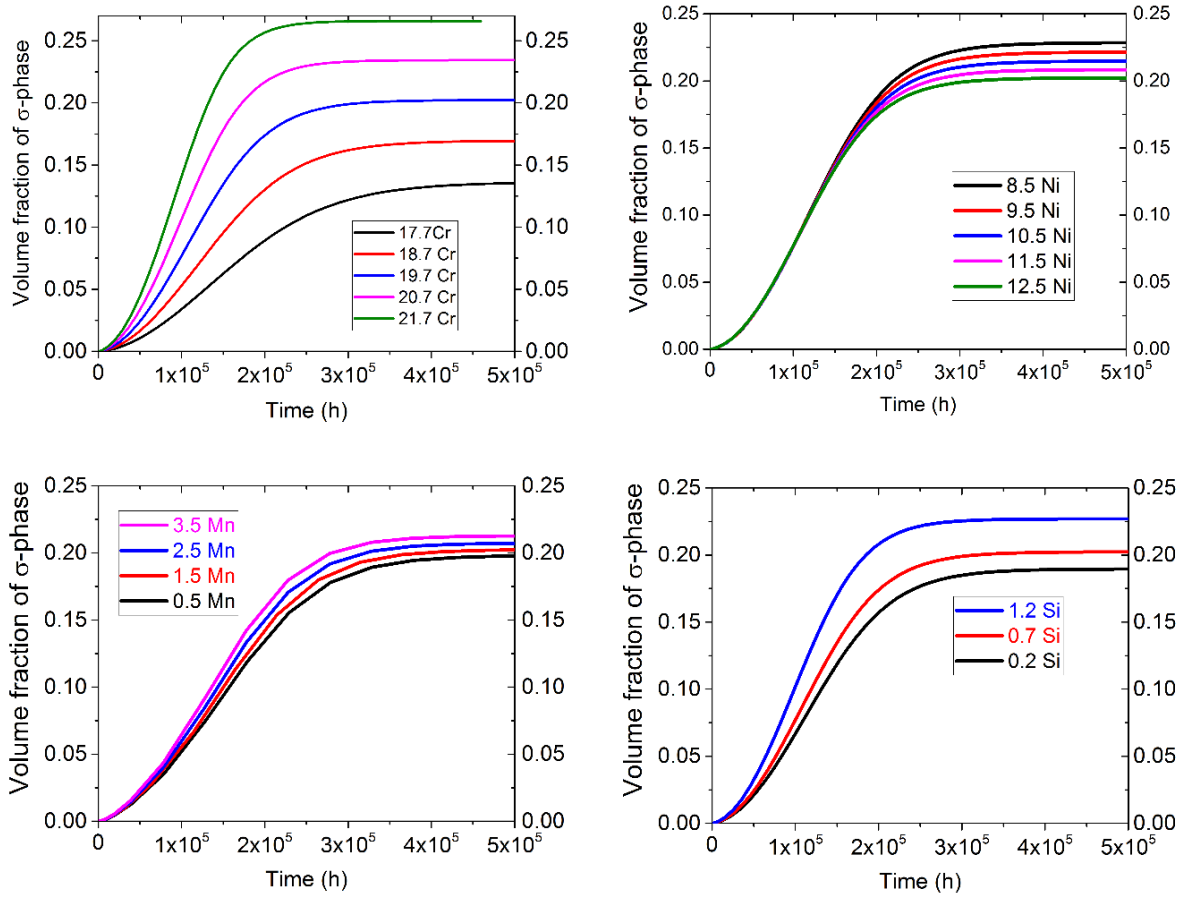

Figure 14: DICTRA simulation showing how variation in composition will influence the volume of the sigma phase at 580°C.

1.5.1.7 Significance of the Ph.D. study

The adverse effect of Cr-rich phases (and thermal ageing) on the corrosion resistance of materials to KCl induced high temperature corrosion has been unequivocally proven in the study. All the studied aged or service exposed materials (with Cr-rich precipitates) showed a remarkably deeper KCl induced corrosion attack compared to the observed attack of the same materials in as received/solution treated condition (without Cr-rich precipitates). Both Cr rich σ-phase and α-Cr were selectively attacked in the aged/heat treated steels/alloys investigated where chlorine was mainly found at the corrosion front which indicates the role of chlorine was more on propagating the corrosion attack. However the increase in volume of Cr rich phases did not lead to increased extent of attack. The attack was primarily due to the Cr composition of these phases, and matrix effects were secondary. Therefore, it can be suggested that the composition of a given phase is the most important parameter to consider, when predicting the response to the chlorine induced corrosion. Hence, by calculating the Gibbs free energy of formation of chlorides of the different chemical elements found in a phase, it is possible to predict the vulnerability of a phase to chlorine induced corrosion. However, the Gibbs free

energy is a thermodynamic property and to better understand the real reaction kinetics such predictions should be supported by experimental investigations.

One of the strategies to reduce the usage of fossil fuels is converting existing coal-firing power plants to firing biomass. The current findings have a line-of-sight implication on converted biomass-firing power plants (which used to fire fossil fuels at higher temperatures). As more Cl-species are released during biomass firing than coal firing, converted power plants could face an accelerated corrosion because of microstructural changes (σ-phase formation) due to precipitation reactions that occurred during service exposure while firing coal. Generally, in the design of materials that are supposed to work at elevated temperatures in KCl bearing environments, the precipitation of Cr-rich phases should be taken into consideration, as such phases can lead to undesirable accelerated corrosion.

1.5.2 WP2 – Corrosion database and models

1.5.2.1 Background to WP2

After organisational changes in the utility companies in Denmark, the collection and comparison at DTU of data from components exposed in biomass fired boilers had come to a halt after 2010 [12]. In the present project investigations have been re-initiated and there has been a continuous (re)-elaboration of previous and new results as well as dissemination of results via published papers, reports to boiler owners and presentations at the steering committee and reference committee. In this report, five specific areas of this work are summarised.

a) Since the presence of precipitates was documented in the Ph.D. project to increase corrosion rates in KCl environments, the presence of precipitates within the actual components was investigated and discussed with respect to fireside corrosion (Section 1.5.2.2).

b) Variable outlet temperatures are a reality for biomass CHP thermal plants where in many cases, only heat is needed and not heat and power. Previously the peak temperature (most frequent temperature) was used for lifetime prediction of corrosions rates as this could be directly related to the corrosion rate, however, this was where there was a narrow variation in temperature. The peak temperature of curves with wide variation in temperature could not be correlated to the corrosion rates (see Figure 15 from Avedøre 2 bioboiler in 2010 [13]). Due to removal of many tubes from many banks at FYV8, where temperature profiles had been collected for the specific tubes, this could be used to get an improved model of corrosion rates with respect to temperature for the 18%Cr10%Ni steels TP347H/347HFG in straw firing environments. (Section 1.5.2.3)

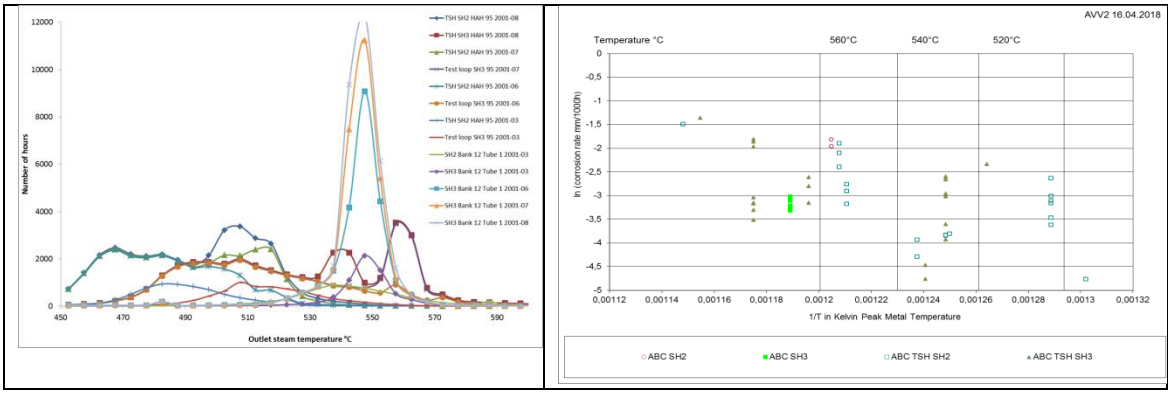

Figure 15: Results from Avedøre 2 bioboiler test superheater from 2010

c) In 2008/2009, two sets of test tubes with the candidate materials in Table 4 were built into two different biomass boilers, a grate fired straw boiler (FYV8) and a suspension fired straw/wood pellet boiler (AMV1), which now only burns wood pellets, Table 5. Due to the mentioned organizational changes, the invaluable comparison of materials needed for materials selection had not been undertaken. (Section 1.5.2.4)

Table 4: Specifications of test tubes in wt.% (bal. Fe)

	C	Cr	Ni	Si	Mn	Nb	Cu	Others
TP 347H FG	0.04-0.10	17.0-20.0	9.0-13.0	<1.00	<2.0	Nb or TaxC<1.00		
DMV347HFG	0.06-0.10	17.0-20.0	9.0-13.0	<0.75	<2.0	8xC<1.0		
DMV304HCu or TX304HB	0.07-0.13	17.0-19.0	7.5-10.5	<0.30	<1.0	0.3-0.6	2.5-3.5	N 0.05-0.12 Al 0.003-0.030 B 0.001-0.010
TEMPALOY AA-1	0.07-0.14	17.5-19.5	9.0-12.0	<1,0	<2.0	2.0<(Ti+Nb/2)/C<4.0	2.5-3.5	B 0.001-0.004
DMV310N	0.04-0.10	24.0-26.0	17.0-23.0	<0.75	2.0	0.2-0.6		Mo 1.10-1.50 N 0.15-0.35

Table 5: Conditions of the two biomass plants used for exposure

Location	Alloys	Fuel	Duration	Exposure time h	Inlet temperature °C	Outlet temperature °C
Fyn 8 (grate fired) SH4 – tube 20 outlet banks 6-13, tube 1 inlet banks 6-13	347HFG, 347H, Tempaloy AA1	Straw	2009–2013	24164	485	560-65 (exposure time max 20401h)
Amager 1 (suspension fired), SH2, tube A in bank 13 and 20, adjacent outlet and inlet	347HFG, Super 304H, 310N	Wood + straw pellets	2009-2014	30534	490-510	540-545

d) Steam oxidation

Although the main work on biomass corrosion has been to look at the fireside, the steamside oxidation should not be ignored. Spallation of steamside oxide can cause blockages. Sometimes the way in which the deposit on the fireside is removed can be quite drastic with the use of explosives but also water jets on hot tubes, etc. This could also result in spallation of steamside oxide which accumulates in the bends (see Figure 16), resulting in blockage, overheating and failure.

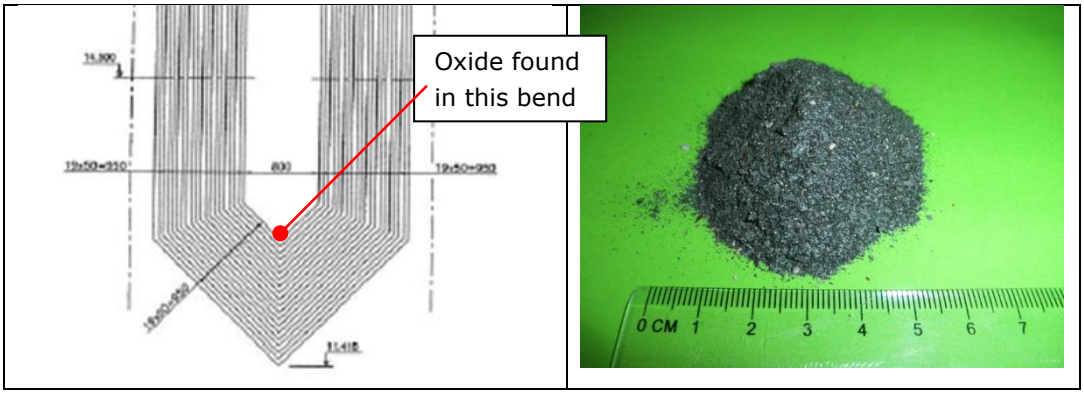

Figure 16: Boiler schematic showing bend and deposit (33g) removed from one bend where there had been a failure

There was a vast amount of data available to this project on oxide measurements from 347H/347H FG and also from shot-peened tubes exposed as described in [19] and this was also compared. (Section 1.5.2.5)

e) As a direct consequence of discussions in the reference group, it was found that in similar biomass plants, problems with repair welding of the vibrating grate had been observed, and also in some cases cracking. This was investigated in depth for for Maribo Sakskøbing [25.

1.5.2.2 Presence of precipitates in service exposed superheaters

As reported in the Ph.D. project when a material is aged, precipitates form within the bulk of the material due to time and temperature. The presence of precipitates was investigated for both Esshete 1250 [14] and 347H/347HFG steel for selected exposed tubes to obtain a better understanding of the formation of precipitates on the fireside of boiler tubes. The observations from 347H are discussed in this section, details of the investigated tubes are in Table 6.

Table 6: Description of 347H/347H FG tubes described in this section.

Sample id	Boiler	Fuel	Steam Temperature	Time (h)
EK9060	Maribo Sakskøbing, SH3	Straw	540	75836
EK9061	Maribo Sakskøbing, SH2	Straw	500	75836
V1088	Fynsværket, bank 5, T1 outlet in penthouse	Straw	545-550	20401
V1089	Fynsværket, bank 5, T1 1 metre from outlet	Straw	545-550	20401
EK8081/EK8084	Avedøre 2 USC	Various Co-firing strategies	Approx. 560C	101100

The tubes with the longest history in a standalone biomass boiler (75836 h from Maribo Sakskøbing) were investigated. Without etching, precipitates were only visible with the scanning electron microscope below the corrosion front at the fireside. Dark precipitates were present about 60µm into the depth of the material as shown by the white arrows (Figure 17) for both superheater 3 (steam temperature 540°C) and superheater 2 (500°C), however they were more visible for superheater 2. These were analysed to be Cr rich, however since they were darker than the matrix in the BSE mode of electron microscopy, it is unlikely they were σ-phase and more likely that they were chromium carbides.

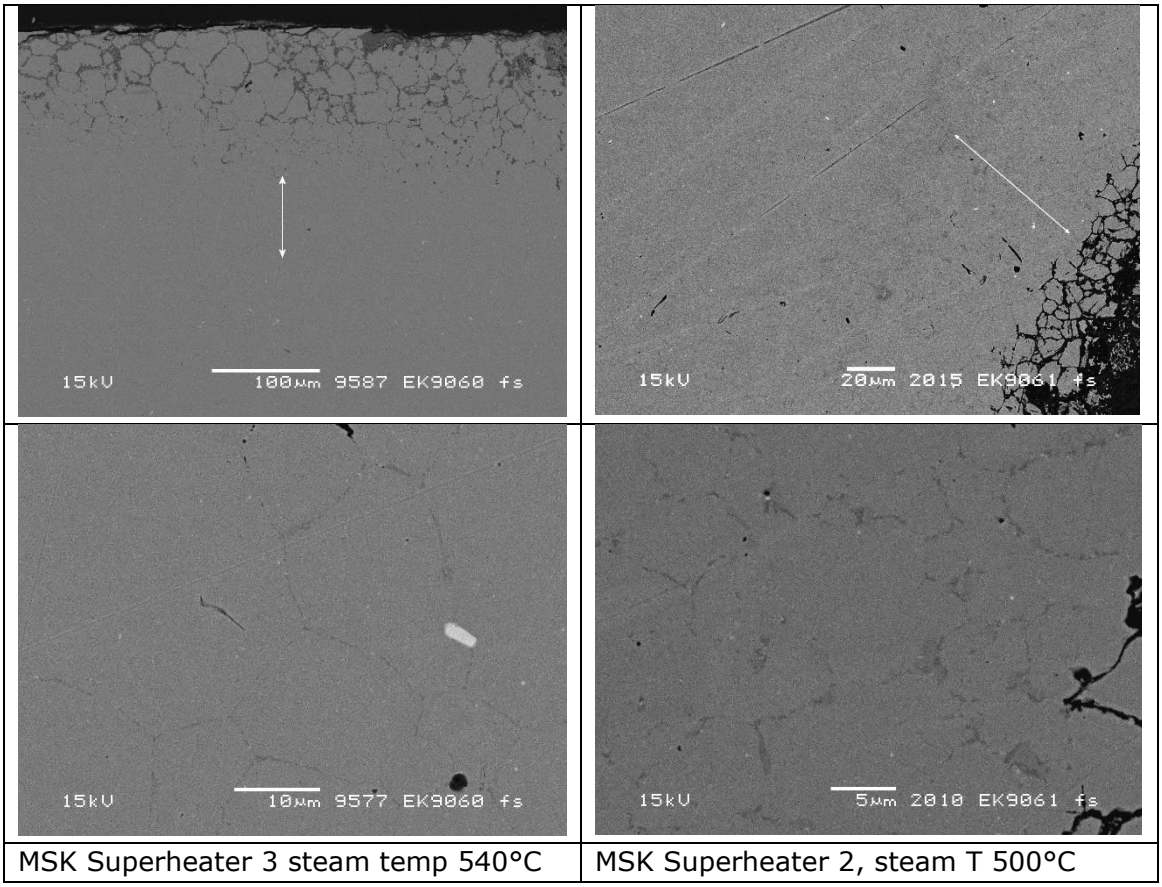

MSK Superheater 3 steam temp 540°C	MSK Superheater 2, steam T 500°C

Figure 17: Tubes of 347H from Maribo Sakskøbing after 75836 h exposure.

To ascertain whether it was only ageing and not also corrosion of the tubes that had some influence on the microstructure adjacent the corrosion front, a tube was investigated which had both a section from the penthouse and a section from the combustion zone (Figure 18). The sections were prepared together such that preparation and etching were the same. The tubes had been exposed to a slightly higher steam temperature than Maribo Sakskøbing varying around 550°C. The tube which was corroded had a higher susceptibility to etching in different etchants such as Murakami, Viella and Kallings (Figure 18) [14]. However the dark precipitates observed in Figure 17 were not obvious for the penthouse section and "white" precipitates (probably NbC), revealed using a gentle glyceregia etch, were present at grain boundaries. On the tube located in the combustion zone, the dark precipitates could be found occasionally (white line across such a precipitate) but were generally absent. A positive identification that they were Cr rich could not be obtained.

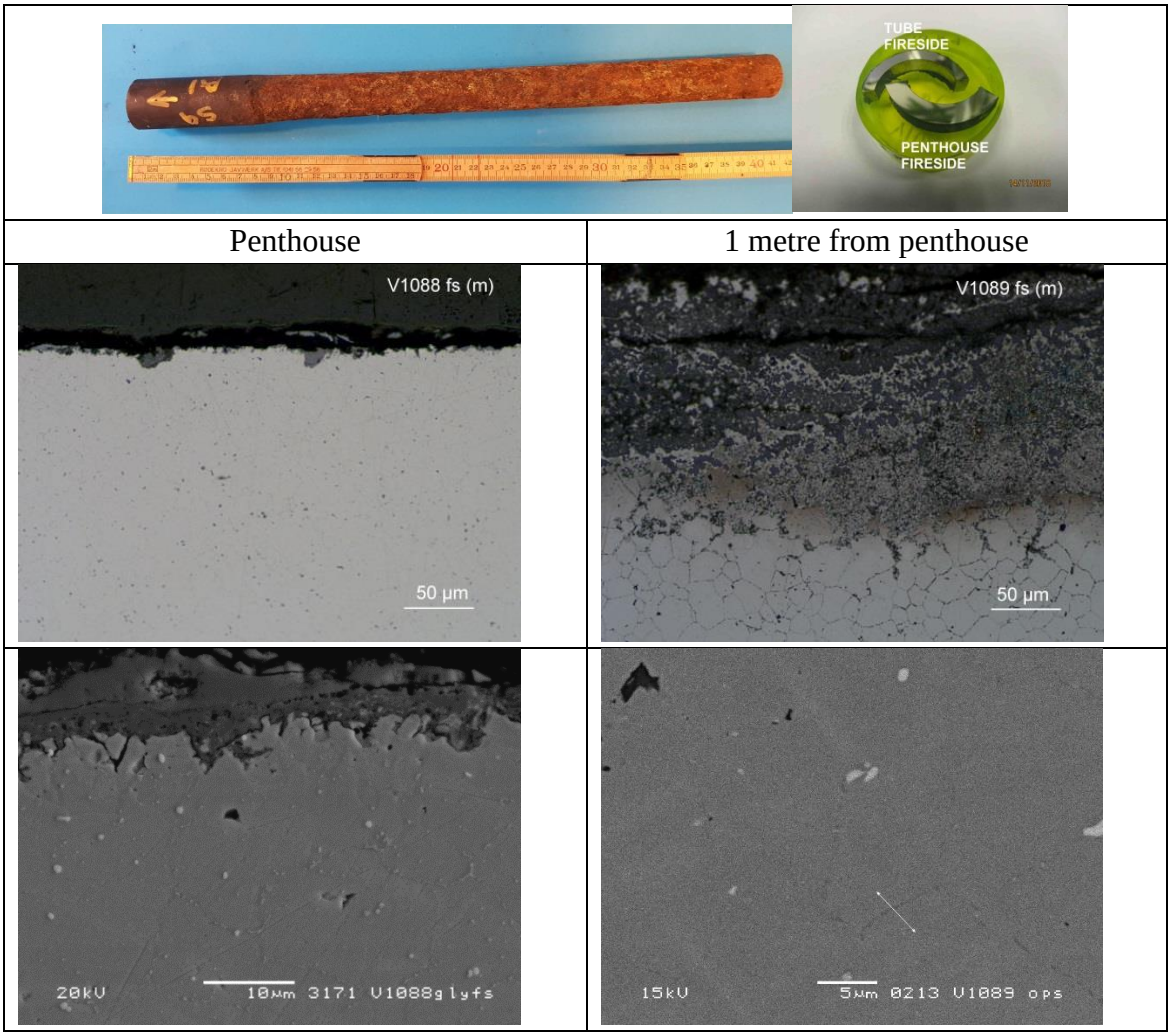

Figure 18: Comparison of microstructure for the penthouse and combustion zone sections.

Thus there were visually two types of precipitates: dark precipitates which may be linked to the corrosion front and light precipitates which are probably linked to ageing in the bulk of the tube. It is to be noted that the tubes experienced lower temperatures and shorter exposure times than the tube from Nordjyllandsværket, where σ-phase was identified (described in section 1.5.1.3.). The question then arises as to whether precipitates at the corrosion front were specifically linked to biomass combustion and KCl corrosion and therefore coal-fired and co-fired tubes were investigated.

It was found that a zone of dark precipitates below the corrosion front was clearly present at the fireside for both co-firing (Avedøre 2 USC boiler) and coal-firing (Nordjyllandsværket) after approx. 100000 h exposure which were 300µm and 100µm wide respectively. The presence of Cr rich precipitates below the corrosion front for both co-firing and coal firing had also been observed for Esshete 1250 [14]. Using a co-firing tube section exposed for 101100 hours more advanced characterisation was undertaken to understand the nature of the dark Cr rich precipitates. Figure 19a shows a light optical micrograph just below the fireside corrosion front where precipitates were present within grain boundaries. A FIB lift-out across a grain boundary was taken close to the corrosion front (Figure 19b).

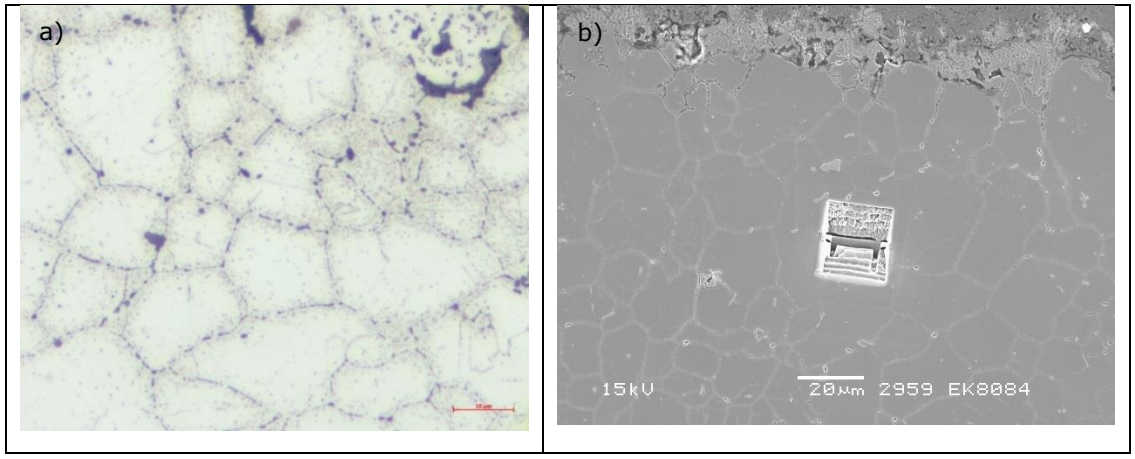

Figure 19: Fireside of the 347H FG tube exposed for 101100 h at Avedøre 2 USC co-firing boiler: a) Light optical micrograph etched with glyceregia showing precipitates below the corrosion front b) and position where FIB lift-out was taken for TEM analysis close to corrosion front on a grain boundary.

TEM analysis (*Figure 20*) of the FIB lift-out revealed large Cr rich precipitates on the grain boundaries which were identified to have the crystallographic structure of $M_{23}C_6$ and based on the EDS results it can be concluded that they are Cr rich $M_{23}C_6$. In addition fine Cr rich $M_{23}C_6$ precipitates were observed within the grains which were more prevalent close to grain boundaries. This is probably the fine particles observed adjacent grain boundaries in Figure 19a.

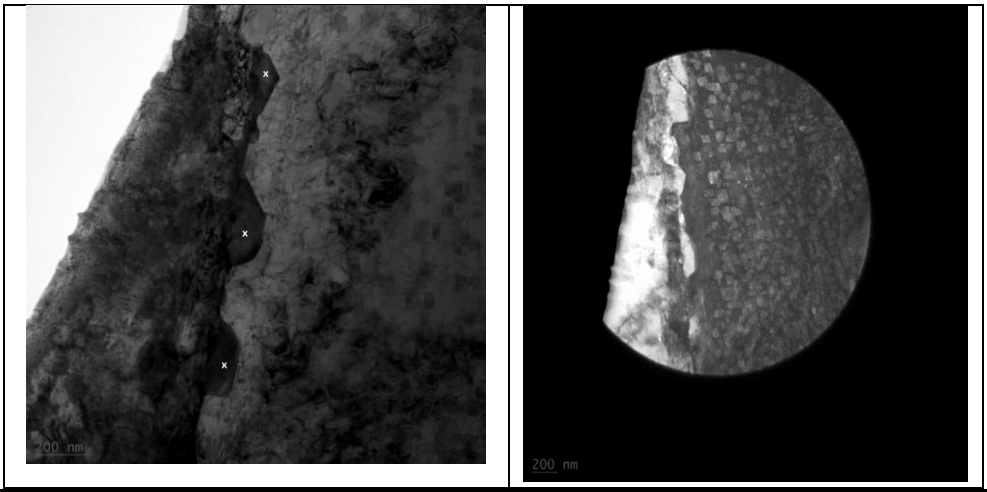

Atomic %	C	Cr	Mn	Fe	Ni	Nb	Mo
Particle 1	20.00	56.17 (70)	1.45	19.10	2.47	0.13	0.67
Particle 2	25.85	56.31 (75)	0.75	13.79	1.98	0.23	1.09
Particle 3	20.32	54.63 (69)	1.44	19.53	2.69	0.79	0.60

Figure 20: a) Analysis of precipitates on grain boundary in atomic % of elements where carbon was present. Cr content in parentheses is when C content is not included. b) TEM DF image revealing Cr rich precipitates within the grain.

To investigate the precipitates in the bulk aged tube away from the corrosion front, the replica method was used. A high number of precipitates were present at grain boundaries as shown in Figure 21 and analysis of 29 precipitates revealed that 65%

were Nb rich (> 70% Nb), 28% were Cr rich (>75% Cr) and 7% of particles were Cr and Nb rich. Since precipitates were removed from the matrix, there is no problem with interaction volume within the matrix. Nb rich precipitates were identified by diffraction patterns as MX particles. The Cr rich precipitates were not identified with diffraction patterns but could be sigma phase or Cr carbides.

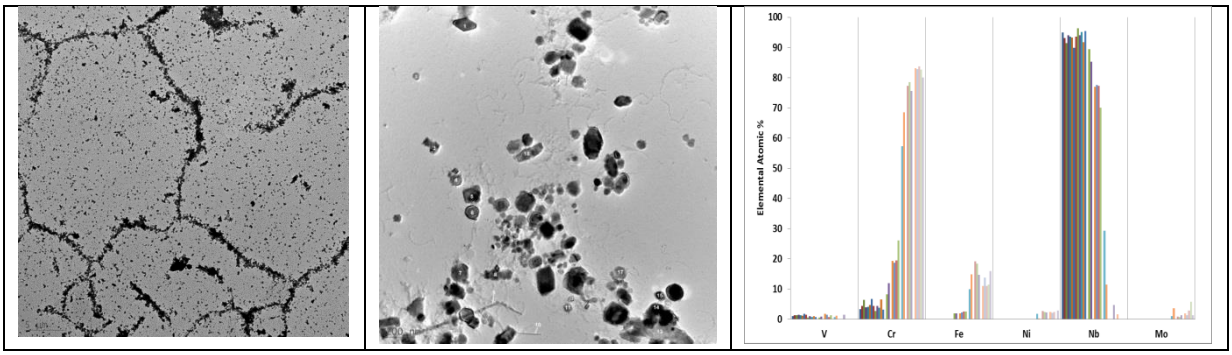

Figure 21: a) and b) Replica of showing majority of precipitates at grain boundaries. c) Elemental composition (without carbon) for analysed precipitates (29 analysed).

Investigation of service exposed components from different plants has shown the presence of precipitates in the steel on the fireside as well as precipitates within the bulk which could be due to different factors:

1. During ageing of steel, the microstructure evolves and precipitates will form at high energy sites such as grain boundaries. This was observed from the Ph.D. work and in Figure 21. For the Ph.D. project, these were found to be large sigma phase particles, however for a component exposed to slightly lower temperatures, the precipitates were smaller and both NbC and Cr rich precipitates were identifies.
2. Dark Cr rich precipitates are formed preferentially at the fireside at the various temperatures and with different fuels. These were identified as $M_{23}C_6$ with TEM. It could be suggested that where there is a higher temperature, precipitates would be more likely to form through faster kinetics; therefore there may have increased presence at the fireside since there is a temperature gradient through the wall thickness. This was clearly the case reported in the Ph.D thesis for the sigma phase in the bulk of the tube on the 0° and 180° side. However this does not seem to be the case here, where the dark Cr rich precipitates are not present at the steamside or in the bulk for components that have higher temperatures.
3. For biomass boilers the presence of the precipitates decreased at higher temperatures, which is probably due to the preferential attack of $M_{23}C_6$ at higher temperatures described in section 1.5.1.5., thus as soon as the $M_{23}C_6$ are formed, then they are attacked. This is not the case for the boilers with lower temperatures (compare Figure 17 and Figure 18).

The formation of $M_{23}C_6$ carbides at the corrosion front could be due to two factors and it is suggested that they are both in play:

1. Where there is preferential attack of primary carbides, NbC, with for example sulphidation or chlorination, then the carbon can be released to form Cr carbides further into the material. It follows that the more corrosion attack there is (which is the case in more sulphidation environments such as co-firing), the more carbon will be released and the greater the carbide zone will be below the corrosion front. This would explain the wider zone present

of $M_{23}C_6$ for co-firing than coal firing which were not linked to the ageing process of the steel.
2. The contribution from carbon dioxide in the flue gas cannot be dismissed and its role needs further investigation.

Figure 22 shows a schematic of the corrosion mechanism in a coal-firing or co-firing atmosphere. In addition to reactions on the surface resulting in iron oxides and alkali sulphates, preferential attack of carbides was observed resulting in grain boundary attack and chromium and manganese sulphides form at the corrosion front. Initially this could be Nb carbides which are in the steel releasing carbon to form Cr rich $M_{23}C_6$ carbides.

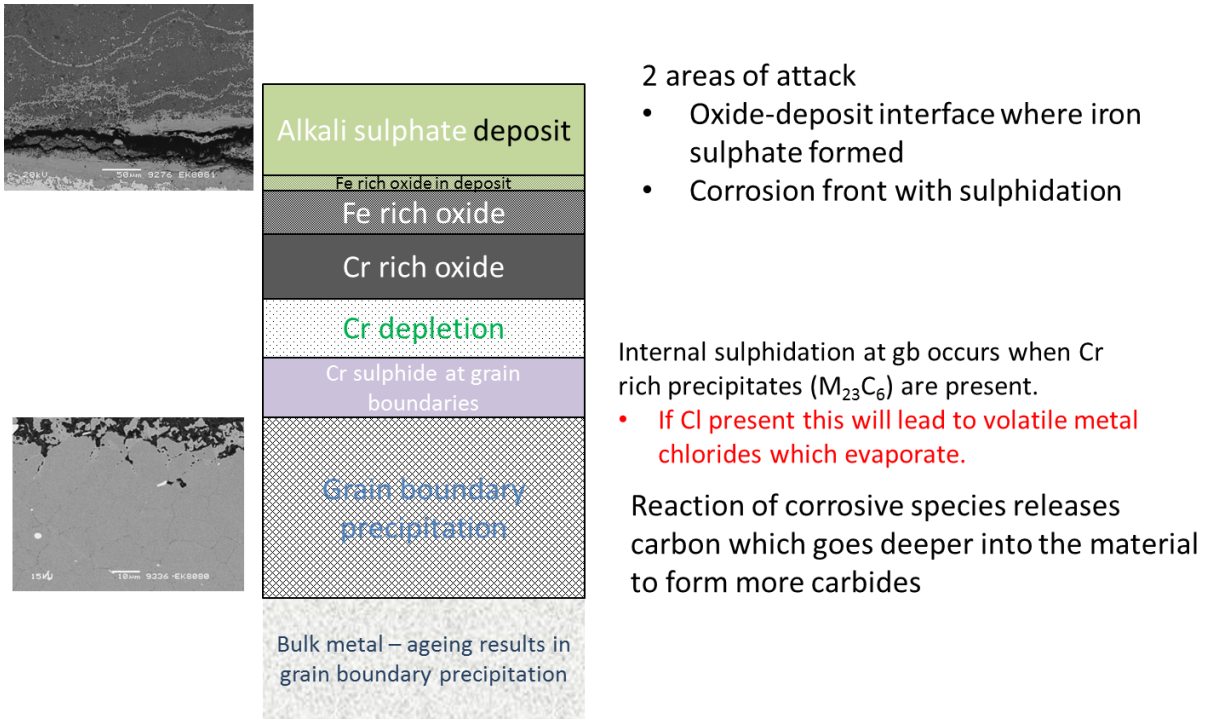

Figure 22: Schematic of corrosion in co-firing and coal boilers.

Similar reactions to those in Figure 22 occur in biomass environments, and as shown very clearly in the Ph.D. work, a preferential reaction of Cr rich precipitates, also Cr carbides, occurs when KCl is present. However these precipitates are not so noticeable in biomass firing, and were difficult to observe with increasing temperatures. It is therefore suggested that the Cl species especially at higher temperatures constantly attack the newly formed carbides resulting in the deep intergranular attack observed.

1.5.2.3 Lifetime prediction

1.5.2.3.1 Comparison of different plants

The 18%Cr-10%Ni steels TP347H/TP347H FG is the most widely used superheater steels in standalone biomass boilers in Denmark and their corrosion has been investigated in a large number of materials samples removed from the boilers, with the longest running samples after more than 75,000 hours at steam temperature of 540ºC.

The overall performance of the steels is shown in Figure 23 by plotting metal loss against exposure time. However, since corrosion varies greatly with temperature or fuel type changes such a plot cannot be used for lifetime prediction, and data have to be refined to derive a model useful for lifetime prediction.

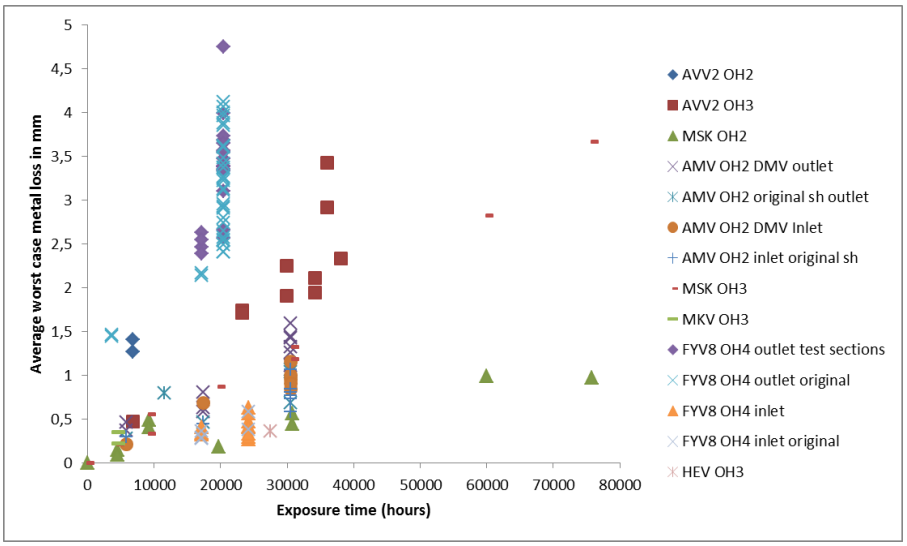

Figure 23: Comparison of results for TP347H/TP347HFG in Denmark.

For the FYV8 and AVV2 bio-boilers, both fired with straw, there are large variations in the available metal loss measurements because of varying temperature during the operation time of the boilers. Thus, these data were removed in Figure 24.

The data from the longest exposure times were from Maribo-Sakskøbing (MSK). Here the outlet temperature had only little variation so a relation can be derived for this boiler for metal loss with respect to exposure time. At the lowest temperature (MSK OH2) with a steam temperature of 500ºC data shows a trend of reducing corrosion rate with exposure time, indicating that some protection is maintained during corrosion. However, the tubes removed from superheater 3 where the steam temperature was 540°C indicate a linear increase in corrosion and no protection can be maintained. This intense corrosion caused by the effects of microstructure changes investigated in the Ph.D project, which become more prevailing at increasing temperature.

The measurements from AMV1 are close to MSK, even though more wood pellets and in recent years only wood pellets were used as a fuel in the AMV1 plant. The present dataset does not allow a direct comparison between a standalone wood fired and straw fired plant at 540°C steam temperature. However, assessment of deposits from a wood and a straw fueled plant (Randers and MSK [17]) revealed that KCl was within the deposit adjacent the tube for both boilers, although to a lesser extent for the wood fueled boiler, and as long as there is a temperature gradient, KCl will continue to migrate in [18]. Therefore the available data suggest that the corrosion rates for wood can be similar to straw firing with grate-fired or suspension fired boilers. This may not be the case for CFB boilers as the flue gas temperatures are lower and may lead to more complete sulphidation of KCl in the combustion zone.

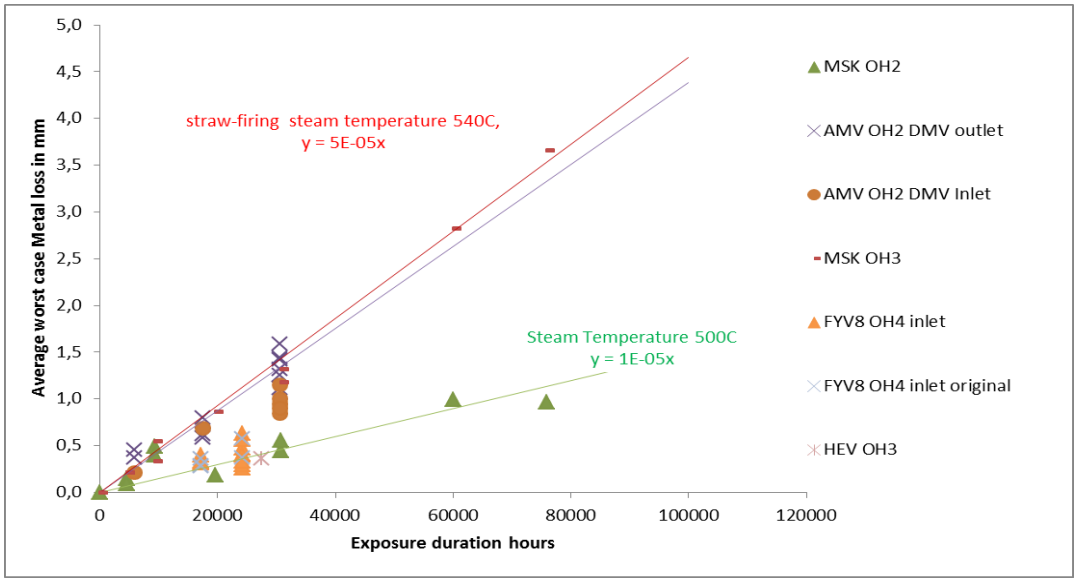

Figure 24: Same data as Figure 23 after removal of FYV8 outlet and AVV2bio data

1.5.2.3.2 Variation of temperature

In some boilers such as Fynsværket, Avedøre 2 bioboiler and Amager 1 the measured temperatures showed great variatin during operation. When using the peak temperatures as a parameter an Arrhenius type plot with an assumed linear corrosion rate is good to compare data from different exposure times and temperatures (if the temperatures are not too variable). The spread in the results is then somewhat reduced, figure 25.

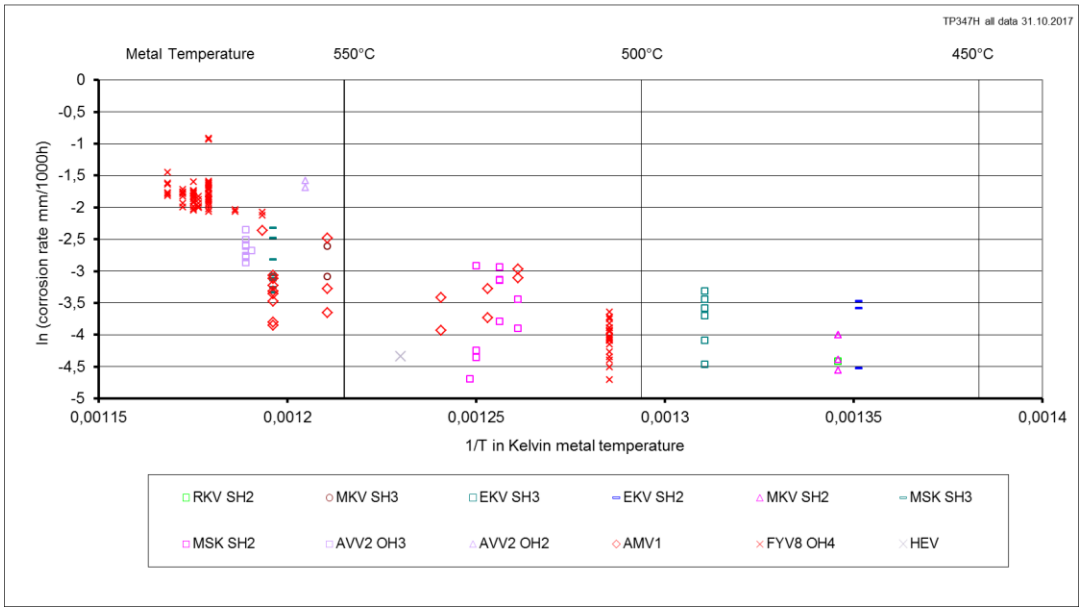

Figure 25: Comparison of data using an Arrhenius plot (average worst case corrosion rate and peak temperature is used)

As previously shown [12], at temperatures above 540°C, the corrosion is extremely fast, therefore it is important to be able to weight the different temperatures experienced by the tube in order to assess how fluctuations in temperature affect corrosion rates. After the failure at FYV8 in 2013, many tubes of 347H/347HFG had been removed, where detailed temperature data had been collected (Figure 26). In the present project the corrosion rates of the components from FYV8 were re-assessed

in order to obtain an improved way to handle data for components with varying temperature profiles.

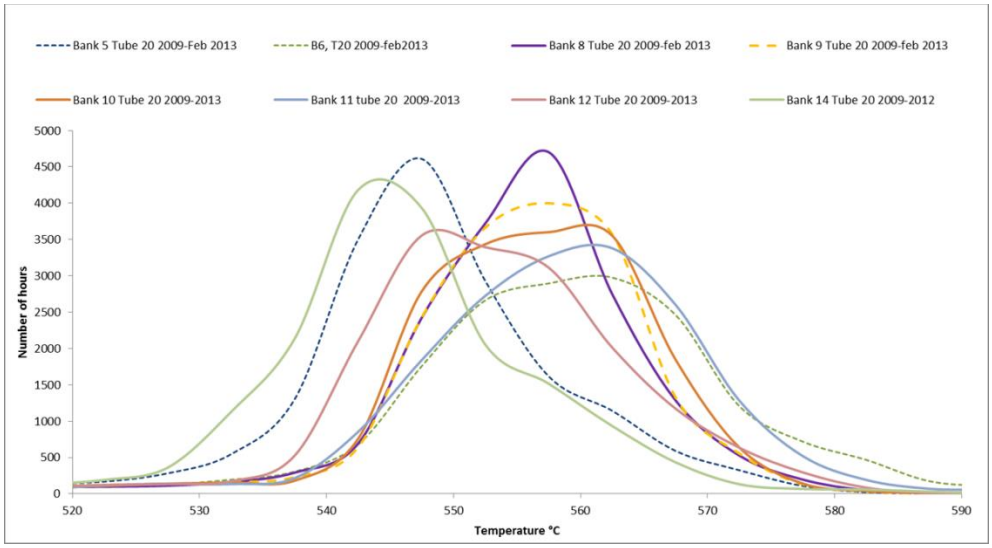

Figure 26: Temperature profiles for the outlet test sections removed from FYV8 in 2013.

Usually the metal loss rates is measured as average worst case (AWC), which is most often the tube thickness loss in the flue gas direction and is what is needed to assess failure. However, corrosion rates for FYV8 boiler close to the outlet vary greatly from one side of the tube to the other (Figure 27). Since the steam temperature measured is relevant for the whole tube circumference, and the extra surface metal temperature comes from the heat flux from the flue gas, then the average best case metal loss (ABC) was used to give a corrosion rate as this would correlate better to the steam temperature measured in the penthouse. Depending on the distance from the outlet, the temperature at the place of investigation was estimated.

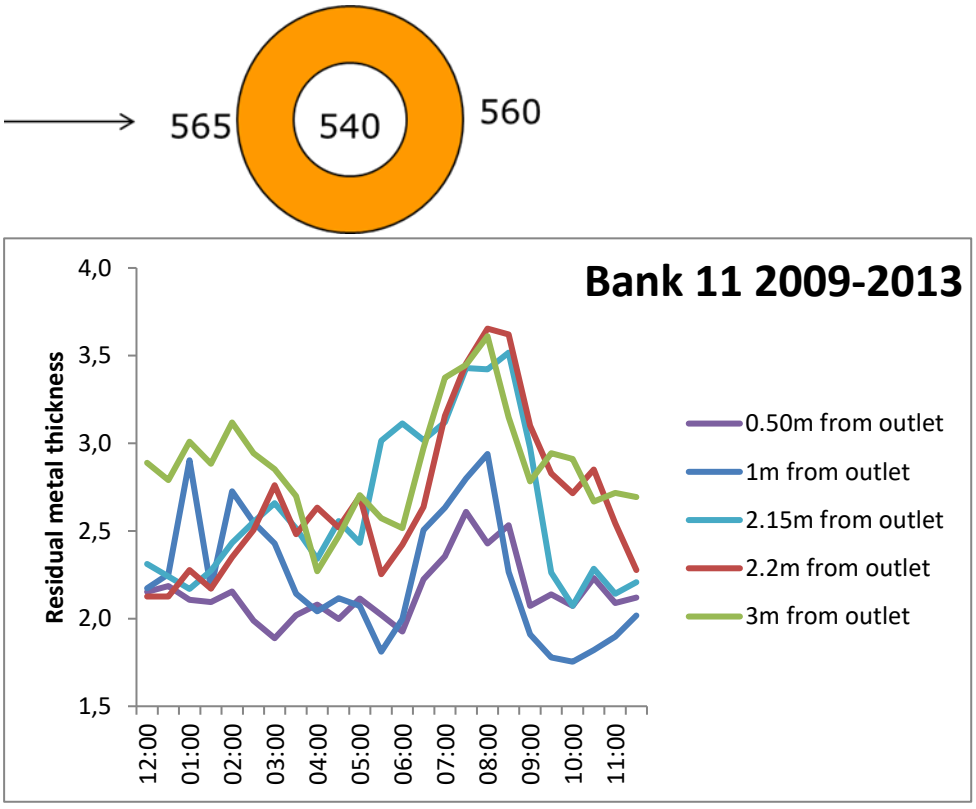

Figure 27: Variation in residual metal thickness around the tube. (12:00) is heading

the flue gas direction.

An Arrhenius type plot was made based on the average best case corrosion rates and an arithmetic mean temperature from the temperature profiles, thus taking into account the temperature variation during operation (Figure 28).

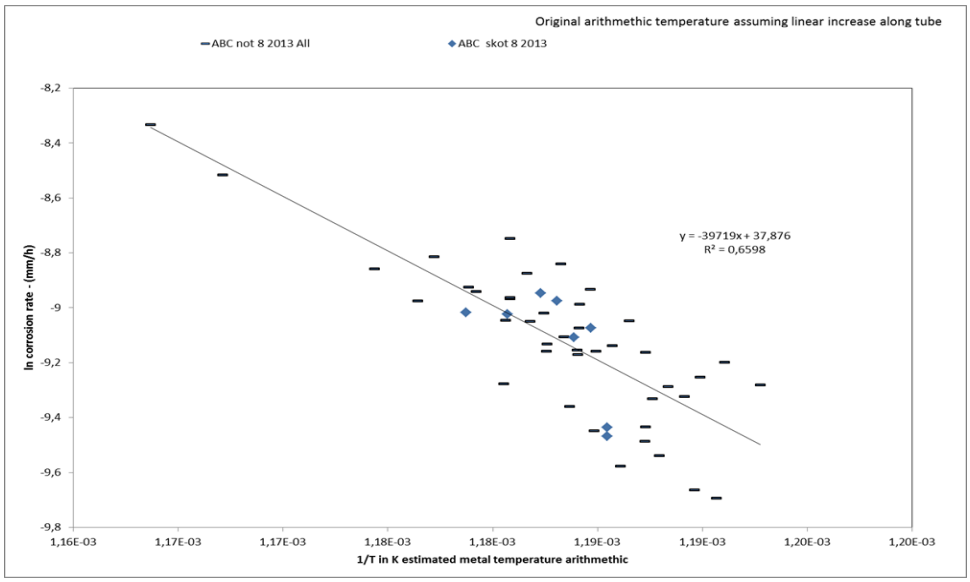

Figure 28: Average best case corrosion rate and arithmetic mean metal temperature used to develop an Arhenius type plot.

The data were then further assessed with the following assumptions:

a) Only sections within approximately 1.5 metres of the tube length were considered, since heat flux is similar in this 1.5 metre tube length on the shielded part (lowest corrosion rate).
b) An increase of 20°C is added to the steam temperature to give surface metal temperature
c) average best case corrosion rates used (previously average worst case)
d) Steam temperature increase over the superheater assumed to be linear between inlet and outlet when assessing temperatures for different sections from the same tube.
e) Both 347H and 347H FG considered together.
f) All tubes had pre-corrosion thickness measurements which were premeasured for test sections, and was the measurement from the penthouse for the original tube. Thus data from 42 tube sections had data that could be used. One bank was excluded as when looking at temperature data it was concluded that it leaked for a month before removal.
g) Initially, arithmetic mean temperatures were used, thereafter metal temperatures were calculated from the temperature profiles in figure 26 using the equation:

$$t_{total}.\ e^{-E_a/(R.T_{metal})} = \sum_{450}^{600} t_i.\ e^{-E_a/(R.T_i)}$$

Where t_{total} is the full exposure time and T_i is the metal temperature in the time interval t_i, and R is the gas constant. The equation was used to fit the activation energy E_a.

After 5 iterations where the calculated metal temperature T_{metal} changed <0.5°C between the 4th and 5th iterations, the E_a activation energy was obtained as **241,5 kJ/mole**, and this indicates how the corrosion rate changes with respect to temperature, and therefore is alloy specific for steels TP347H/TP347HFG in this environment, i.e. straw firing.

Previous work had shown that it had been difficult to show a trend between corrosion rates and temperature for tube specimens from the Avedøre bioboiler (Figure 15) since the temperatures had been too variable. At that time, peak temperature and average worst case corrosion rates were used. By taking the average best case corrosion rates and the metal temperature calculated using the activation energy **241,5 kJ/mole**, the Arrhenius plot is shown in Figure 29

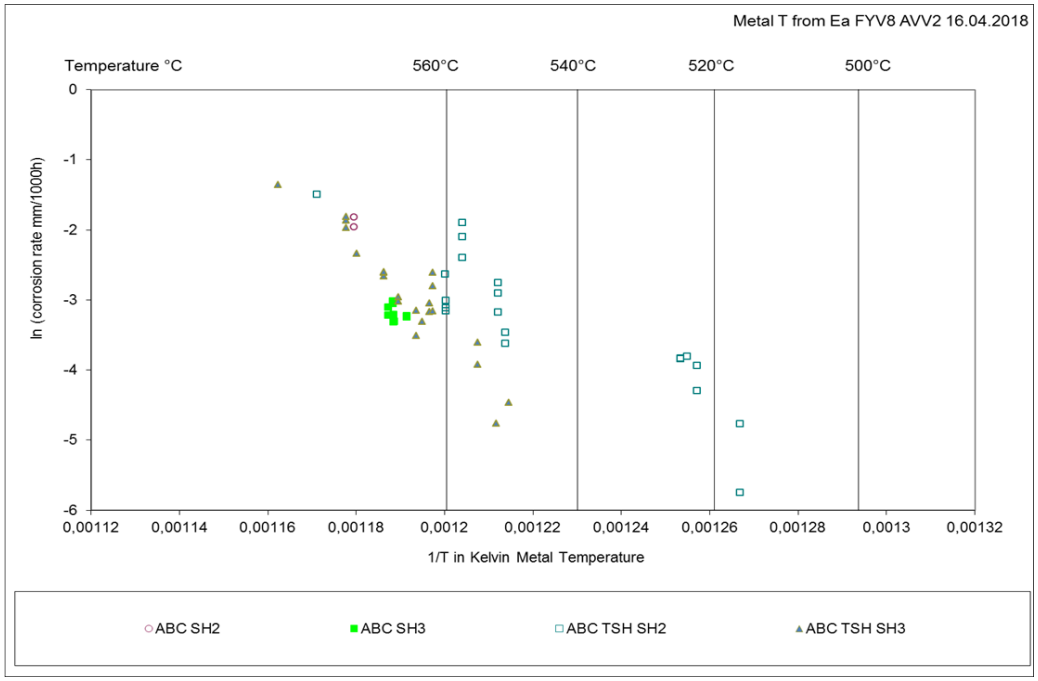

Figure 29: Replotting of data in Figure 15 using calculated T metal and average best case corrosion rates.

With further assessment of increased flux over the combustion zone individual temperature additions of SH2 +25, TSH2 +30, TSH3 +25 and SH3 +20 degrees were used, however such an assessment has to be based on knowledge of heat flux patterns within the boiler. Assessment with respect to precise location from the outlet is not yet incorporated into this analysis, however a clear trend can now be observed.

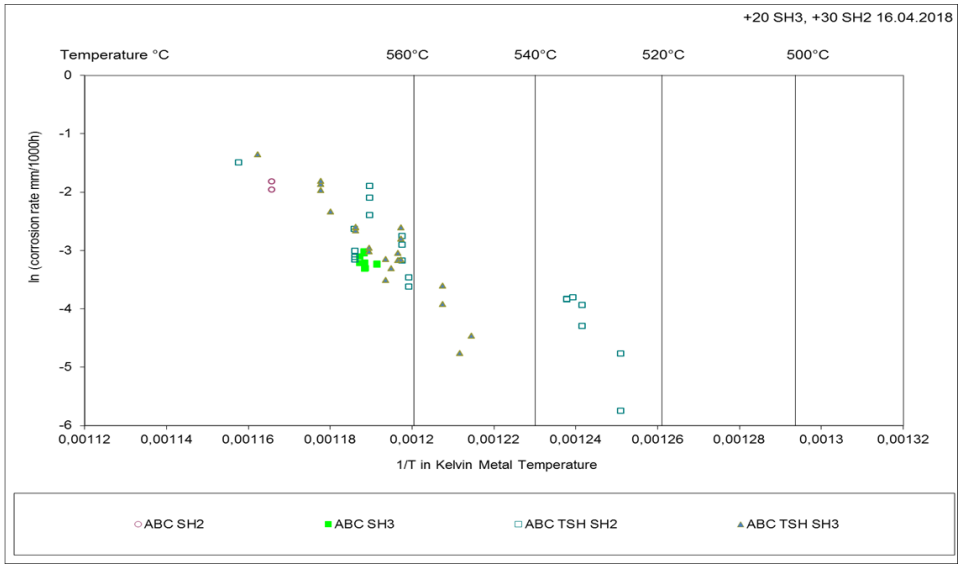

Figure 30: Revised Arrhenius plot with specific assessments associated with location of tubes.

Thus, a basic model for the corrosion rate of steels TP347H/TP347HFG in straw firing is derived from the data as:

$$Kp\ (mm/1000h) = 8{,}84*10^{12}\ exp(-29004/T_{metal})$$

The model predicts a linear corrosion rate in mm/1000 h based on the surface *metal* temperature (in degrees K) at the location of interest, see figure 31. The model is useful both for the estimation of local surface temperature at a point of inspection and for estimation of corrosion rate in design or lifetime prediction for superheaters.

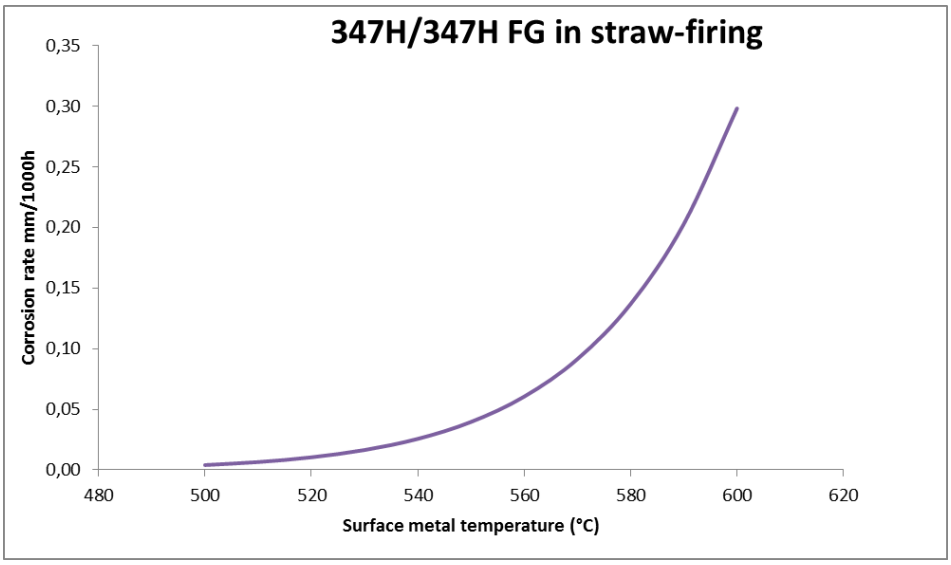

Figure 31: Graph showing the derived basic curve for the corrosion rate of steels 347H/347HFG with respect to temperature in straw firing.

1.5.2.4 Materials selection

One of the goals of this work was to compare new materials in test sections exposed at Amager 1 and FYV8 (Table 4 and 5). Tubes were removed from Amager 1 after 5000 h, 17440h and 30534 h. The results from the latter two exposure durations are shown in Figure 32, however it should be noted that the temperature was slightly higher in the first 17440h, as after this, the plant started to bypass the turbine. At the inlet where there is high heat flux the steam temperature was 500-513°C, the alloy 310N has the best performance, however in the outlet leg where the steam temperature was 542°C in the first 17440 hours but reduced to 539°C for 30534h, the alloy 310N had the highest corrosion rate. The other steels tested had similar corrosion rates. There were two suppliers of Super 304H (A and B), but there was no notable difference in performance of the two variants at the high temperatures.

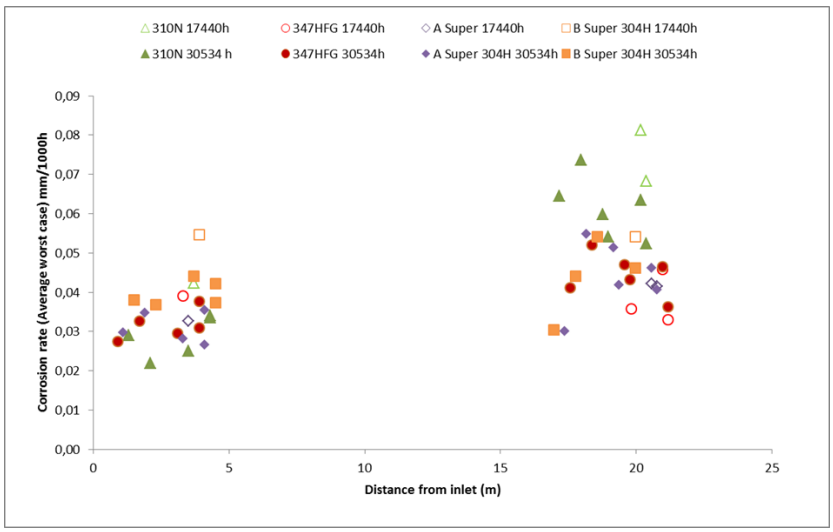

Figure 32: Corrosion rate at AMV1 test sections with respect to location of tube from inlet.

The high corrosion rate of the 310N steel has a great effect with respect to lifetime prediction (Figure 33) and an Arrhenius plot would have a steeper gradient.

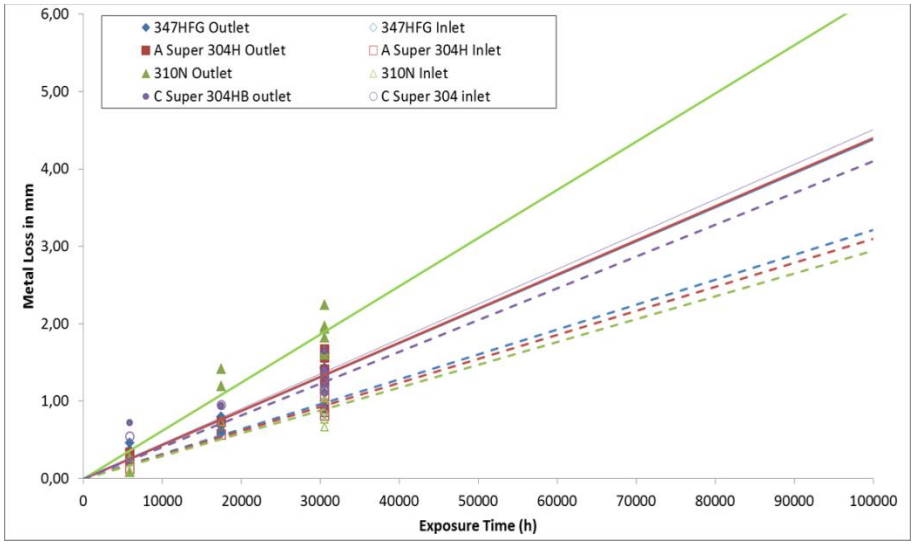

Figure 33: Extrapolated data for steels exposed at Amager 1 test sections.

A range of alloys were also tested at FYV8, where there were four 347H/347HFG variants and a new candidate alloy Tempalloy A1. They were exposed in different banks with the different temperature profiles shown in Figure 26.

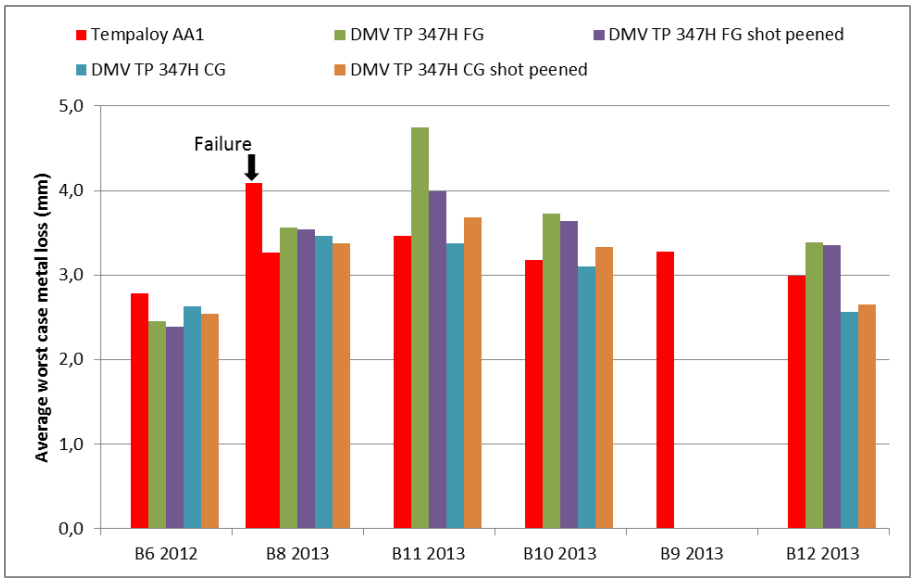

Figure 34: Comparison of test steels exposed in FYV8.

Figure 34 shows the metal loss for tubes from the FYV8 testing. There were slight variations from bank to bank, which could be due to the varying temperature profile and heat flux, however Tempaloy A1, which had similar corrosion rates as the other steels, failed at a thickness of 1.7 mm. It is to be noted that TP347H FG in bank 11 had a residual thickness of 1 mm without failure. This could be linked to the precipitations within the Tempaloy A1 steel as the failure was intergranular.

1.5.2.5 Steam oxidation

As mentioned earlier, steam oxidation is also important as spallation of steamside oxide can lead to blockage and failure as well as to carry over of debris to the turbine. From the extensive amount of data from Danish power plants, a comparison was made of 347H FG and 347H (Figure 35). A comparison of data for TP347H reveals that there are similar oxidation rates for fine grained steels and coarse-grained at the lower metal temperature range (<560-580ºC). In addition the morphology of the oxide is similar and there is no sign of a chromium rich layer which would reduce oxidation [19]. Thus chromium is not mobile in this temperature range. At the higher temperature range (>580ºC), the TP347H FG shows a more protective behavior as the chromium is mobile and can use the fine-grained structure to give increased diffusion to the oxide-metal interface. This results in a chromium rich oxide at the metal-oxide interface. There is no evidence that pressure affects the oxidation rate. Variations in oxidation can also be due to different alloy batches, unintentional surface deformation, and varying temperatures.

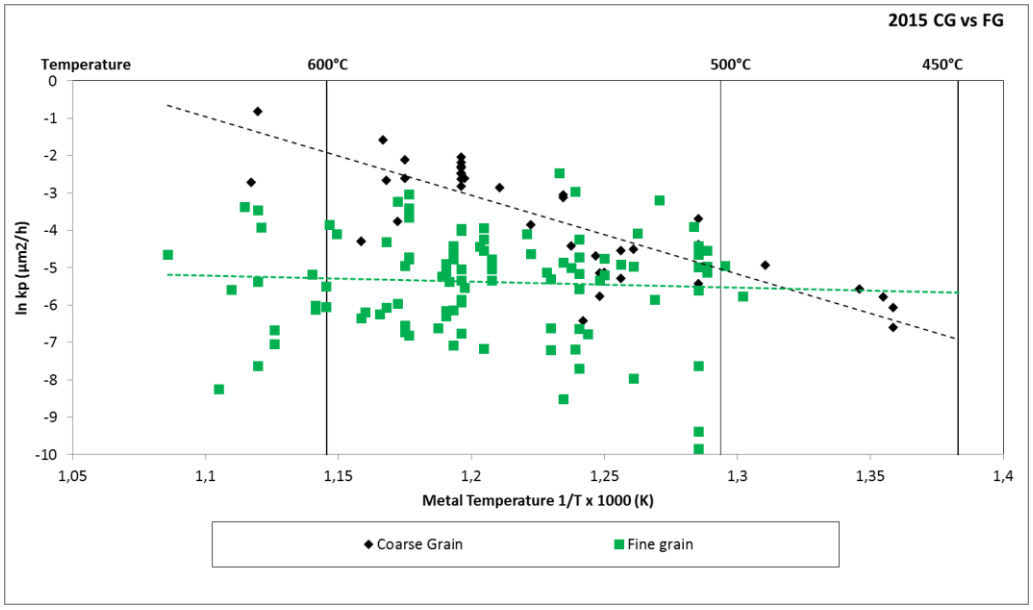

Figure 35: Comparison of inner oxide growth rate for 347H and 347H FG.

Intentional surface deformation i.e. shot peening was investigated for the steels exposed in both boilers. Steel type 347H, 347H FG, Super 304, Tempalloy AA1 and 310 in all cases resulted in a thin oxide which was less than 1 µm, also at low temperatures of 490°C steam temperature. For the tubes exposed for the longest time, there was no sign that the deformed structure had recovered and would lead to slower Cr diffusion rates and therefore a thicker oxide (Figure 36). However, Cr rich precipitates had formed within the lower part of the deformed surface, probably also due to high Cr diffusion.

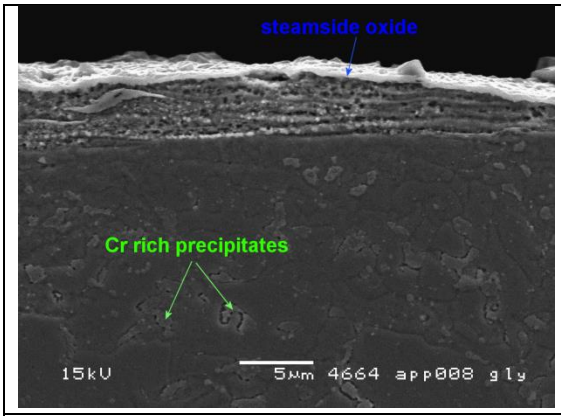

a) 347HCG exposed for 17740 h at steam temperature 550-565°C

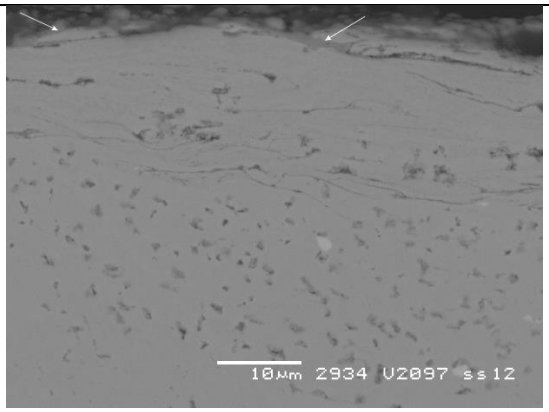

b) 347H FG exposed for 30534h at steam temperature 539°C

Figure 36: Steamside oxidation after shot peening of 347H steels exposed in test sections.

1.5.2.6 Nitridation of the grate in biomass plants

Problems were encountered when repair welding the vibrating 15Mo3 grate at Maribo Sakskøbing. Similar problems had also been observed at Avedøre bioboiler some years ago which had 13CrMo44 grate tubes with 15Mo3 fins. A 15Mo3 piece of the grate from another biomass boiler was also investigated for comparison. The surface metal temperatures of grates are 300-400°C and therefore not so vulnerable to high temperature corrosion.

Table 3: Alloy specification of sections investigated in wt.%

	C	Cr	Mo	Si	Mn	Fe
13CrMo44	0.08-0.18	0.70-1.10	0.40-0.60	0.10-0.35	0.40-1.00	rest
15Mo3	0.12-0.20		0.25-0.35	0.10-0.50	0.40-0.90	rest

At Maribo Sakskøbing the grate had an estimated surface metal temperature of 350ºC and therefore much lower than superheaters previously described, and corrosion attack was slower due to the lower temperature, however the exposure time had been over 93000 hours. Measurement of hardness profiles across the tube wall indicated that the grate tube had a higher hardness at the side closest to the combustion zone (Figure 37). The microstructure was also different in that needle shaped precipitates were present close to the combustion zone and their presence gradually decreased closer to the steamside (Figure 38). In addition, the usual surface hematite and inner magnetite was not always present. Instead the presence of FeOOH (goethite and lepidocrocite) was detected.

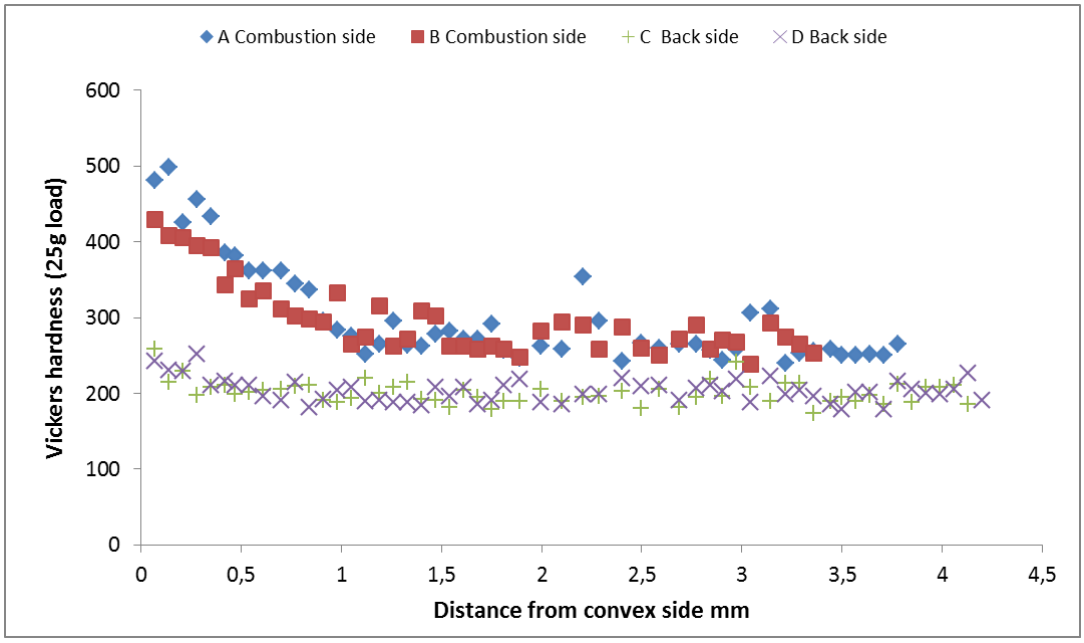

Figure 37: Hardness measurements comparing the combustion side and the backside of the tube.

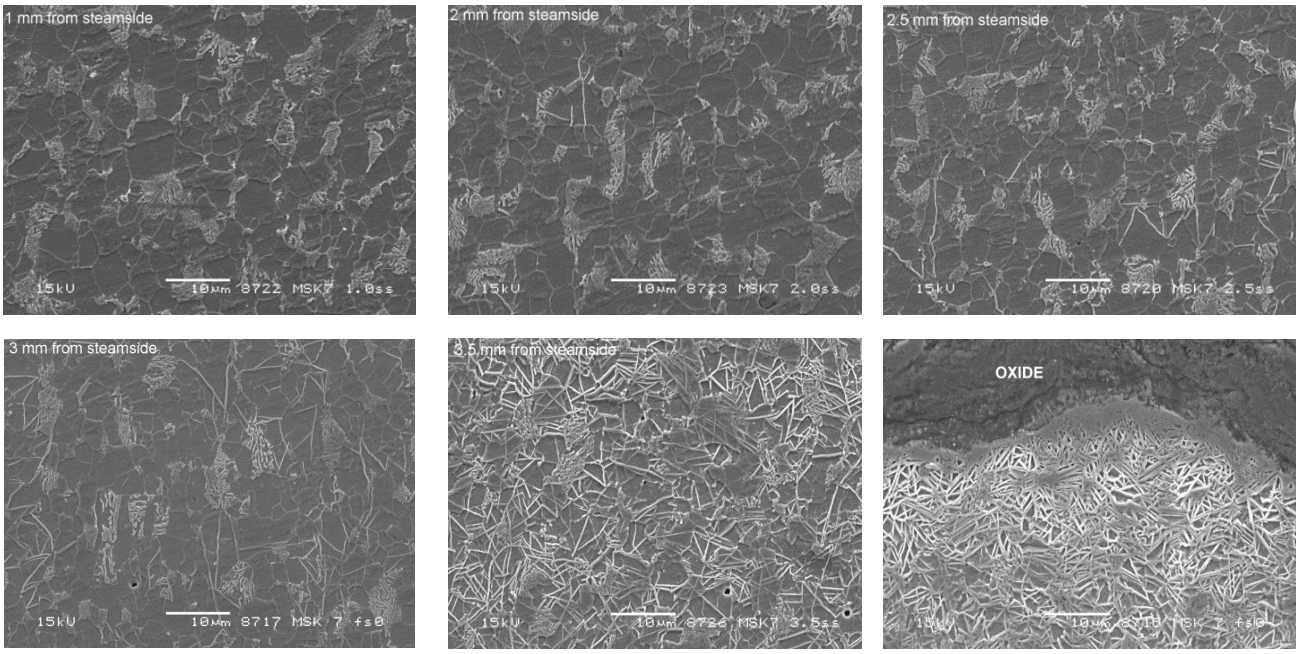

Figure 38: SE micrographs of microstructure on the combustion side showing variation with distance from steamside.

Using advanced microscopy and analysis methods, nitrogen was revealed to be present. Nitrogen is difficult to make a positive analysis, so nitrogen bulk analyses within the tube wall on the side adjacent the combustion side and the backside were undertaken (Figure 39): There was a 10 fold increase in nitrogen on the combustion side.

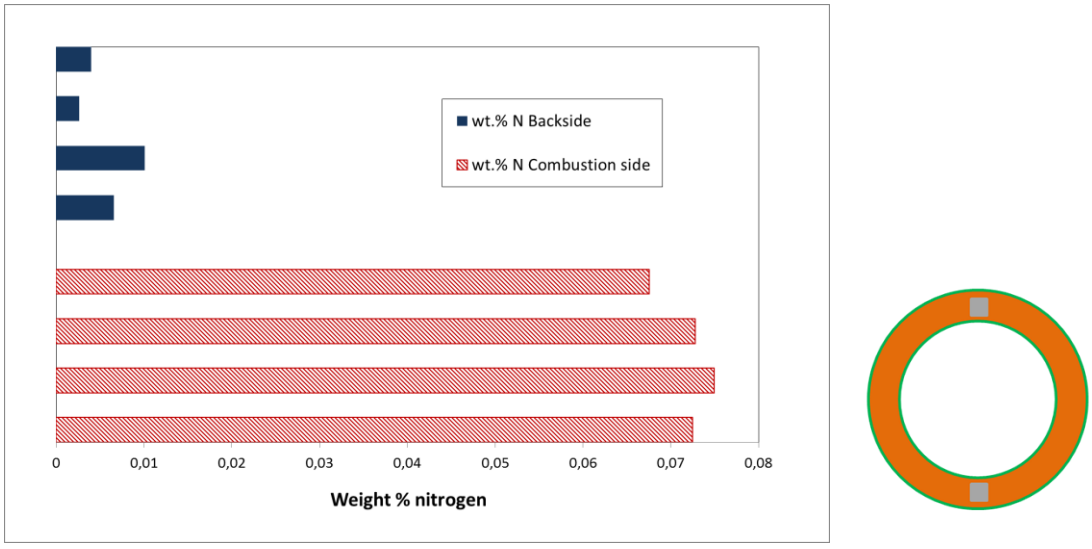

Figure 39: Comparison of nitrogen content from the combustion side to backside of tube on grate. The schematic shows that analysis was in the bulk of the tube.

The evidence pointed to the presence of iron nitride, and that due to the combustion on the grate, NH_3 had formed and before being oxidised to NOx gases had reacted with the 15Mo3 alloy [20]. It had not been previously envisaged that such a reaction would occur at such low temperatures, however the long exposure time in this environment resulted in changes in the tube microstructure/composition. When repair welding was performed, the heating of the Fe_4N surface led to an unstable melt pool as Fe_4N is not stable at temperatures >700°C and would lead to outgassing. A section from the 16Mo3 grate from a straw fired boiler exposed for 55000 h

also showed increased hardness and a similar microstructure to the section from Maribo Sakskøbing.

Analysis of the 13CrMo44 grate tubes from the AVV2 bioboiler revealed higher hardness (than for the 15Mo3 and 16Mo3 tubes) (Figure 40). Three sections from different zones on the grate were investigated to see if location on the grate influenced the profile. All zones had different measures of hardness and these also varied around the tube. Even two tubes adjacent each other had different hardness profiles. In comparison, the fins which were 15Mo3 had hardness values similar to 15Mo3 previously measured from the other boilers.

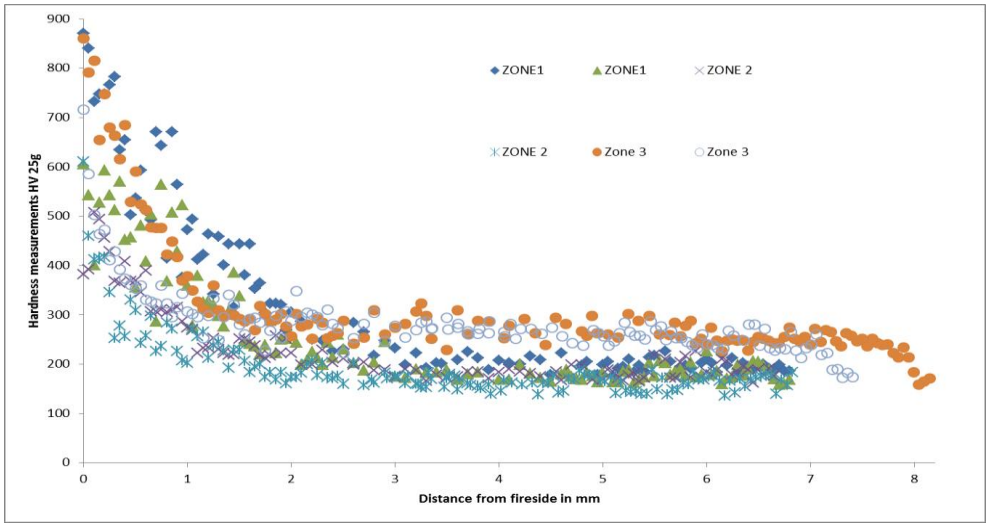

Figure 40: Hardness profile through 13CrMo44 grate tubes from Avedøre bioboiler

Although acicular precipitates were present closer to the surface, darker areas along grain boundaries were also observed (Figure 41). In addition intergranular cracks were apparent, and there had been several failures previously. Based on the extensive investigations of the Maribo Sakskøbing grate, it is concluded that the high hardness is due to nitridation. The cracks were not necessarily present in areas with comparatively higher hardness and it was concluded that it is not the increased hardness that leads directly to cracking but it could be that certain areas are subjected to greater mechanical stresses, which result in the intergranular brittle cracking because of nitridation.

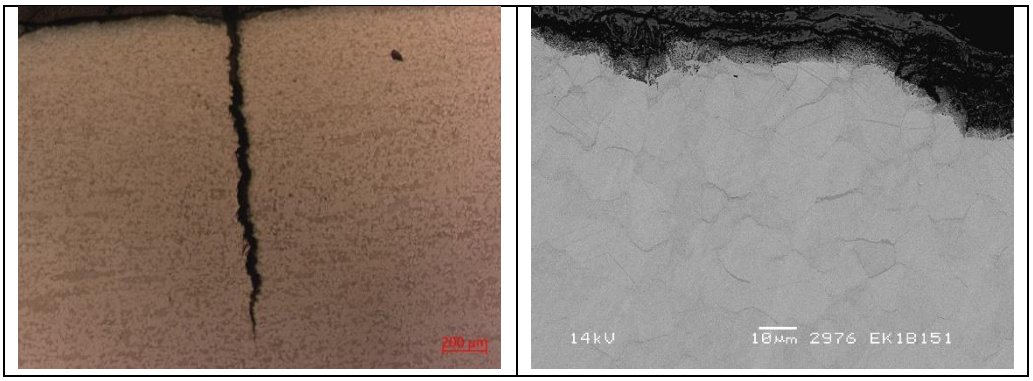

Figure 41: a)Light optical microscopy of partially cracked area and b) scanning electron micrograph image of the microstructure.

The higher hardness compared to that observed for 15Mo3 both in the fins of the grate, and also in other 15Mo3 grate tubes must be due to the increased amount of Cr and Mo in the steel which both have a higher affinity for nitrogen than iron. The presence of Cr may lead to Cr nitrides at the grain boundaries resulting in a greater embrittlement, however this was not proven.

1.5.2.7 Dissemination of results
The project results were disseminated directly to the project partner through five steering group meetings with DONG Energy/Ørsted and DTU Mekanik.

Furthermore, a reference group of Danish operators of biomass fired heat and power plants was organised. This group held four annual meetings during the project, where project results were presented, and the operators presented and discussed experiences related to corrosion at their own plants.

During the project DTU made 27 publications related to Biomass corrosion management, 19 were international publications, see Annex. The publications contained results of the present project as well as unpublished results from previous investigations

1.6 Utilization of project results

Ørsted will use project results directly to optimise the operation of their biomass fired heat and power plants and to choose cheaper materials for replacement components due to corrosion.

The published corrosion models will be used by plant operators and consultants to make life assessments of biomass fired heat and power plants.

Thus, the results developed by university research will be transferred to companies active in biomass corrosion allowing them to better manage biomass corrosion.

The overall objective for the Danish energy policy to replace fossil fuels by CO_2 neutral fuels such as biomass will be facilitated and less costly due to the project results.

DTU will use the results in their teaching as well as to formulate new research related to the corrosion mechanisms discovered in the project.

No patents will be taken.

1.7 Project conclusion and perspective

The overall goal of the project was

- To improve the fundamental understanding of the influence of materials microstructure on the corrosion performance during long-term operation in biomass firing
- To develop quantitative models of corrosion rates as a function of material and corrosive environment

The first goal of the project was realized in a ph.d. project, which unequivocally showed that precipitation of Cr rich phases such as Cr-carbides, sigma phase and

alpha-Cr in steels an Ni base alloys leads to accelerating corrosion caused by direct corrosion attack of the precipitated phases.

This result reveals the previously unknown mechanism for internal corrosion in biomass firing and explains why steels with increasing Cr content higher than 18% shows more intense internal corrosion: They are simply more prone to formation of Cr rich phases.

Experience at grate fired Danish heat and power plants had shown the grates became brittle and lost weldability during long-term operation. Investigations in the project revealed that this was caused by nitridation of the grate surface due to the local chemistry at the surface.

To realize the second goal, a large set of investigation reports from previous collaboration between DTU and Danish biomass fired heat and power plants were collated into a database. Analysis of the data led to the formulation of a general model for corrosion in straw firing as a function of metal temperature.

The results of influence of materials microstructure on biomass corrosion are highly useful for the rebuilding of existing fossil fired plants to biomass firing, since it demonstrates that long-term operation resulting in a change of the materials microstructure leads to poorer corrosion performance. Further the results can be implemented to choose cheaper materials in future replacements of corroded parts in biomass fired plants.

The developed corrosion model is highly useful for the life assessment of superheaters and may lead to savings by avoiding loss unforeseen plant outages due to superheater corrosion as well as to optimum replacements of superheaters due to corrosion.

1.8 References

1. M. Montgomery, A. Karlsson, "*In-situ Corrosion Investigation at Masnedø CHP Plant – a Straw-fired Power Plant"* Materials and Corrosion 50 (1999) p. 579-584.
2. Saeed Kiamehr, "*Material Solutions to mitigate the alkali chloride-induced high temperature corrosion*" Ph.D. Thesis, DTU Mechanical Engineering, November 2014.
3. Sunday Chukwudi Okoro "*High temperature corrosion on biodust firing*" Ph.D. Thesis, DTU Mechanical Engineering, June 2016.
4. Duoli Wu "*Corrosion resistant coatings for biomass firing*" Ph.D. Thesis, DTU Mechanical Engineering, February 2018.
5. M. Montgomery, S. Kiamehr, K.V. Dahl Proceedings "*Danish Experiences in Biomass Corrosion and the Way Forward"*: EPRI International Conference on Corrosion in Power Plants. EPRI, Palo Alto, CA: 2015. 3002006972
6. T. Jonsson, J. Froitzheim, J. Pettersson, J. E. Svensson, L. G. Johansson, and M. Halvarsson, "*The influence of KCl on the corrosion of an Austenitic stainless steel (304L) in oxidizing humid conditions at 600°C: A microstructural study*," Oxid. *Met.*, vol. 72, no. 3–4, pp. 213–239, 2009.
7. S. Kiamehr, K.V. Dahl, M. Montgomery, M.A.J. Somers, *KCl-induced high temperature corrosion of selected commercial alloys: Part I: chromia formers* Mater. Corros. 66, 12 (2015): p.1414-1429
8. Y.C. Malede, M. Montgomery, K.V. Dahl, J. Hald, "*Effect of microstructure on KCl corrosion attack of modified AISI 310 steel"* Mater. High Temp. 35, 1-3 (2018): p. 243-254.
9. Y.C. Malede, J.P. Simon, T. Jonsson, M. Montgomery, K.V. Dahl, J. Hald: *"KCl induced corrosion of Ni-based alloys containing 35-45 wt% Cr*". Materials and Corrosion 2019 prepublication preprint DOI: 10.1002/maco.201810658
10. J.-O. Andersson, T. Helander, L. Höglund, P. Shi, and B. Sundman, "Thermo-Calc & DICTRA, computational tools for materials science," *Calphad*, vol. 26, no. 2, pp. 273– 312, Jun. 2002.
11. A. Borgenstam, L. Höglund, J. Ågren, and A. Engström, "DICTRA, a tool for simulation of diffusional transformations in alloys," *J. Phase Equilibria*, vol. 21, no. 3, pp. 269– 280, May 2000.

12. M. Montgomery, S.A. Jensen, U. Borg, O. Biede, T. Vilhelmsen: *Experiences with high temperature corrosion in straw firing power plants in Denmark*, *Mater. Corros.* 62 (2011): p. 593-605.
13. M. Montgomery, Søren Aa. Jensen, Ulrik Borg "Corrosion Investigations at Avedøre Biomass fired boiler Part IV, December 2010
14. M. Montgomery, K.V. Dahl, S.A. Jensen, C. Davies: **"***High Temperature Fireside Corrosion of Esshete 1250 in Coal, Co-firing with Biomass and Biomass Power Plants".* Proceedings Eurocorr 2017, Prague 3-7th September, 2017.
15. KME report 714: Sulfur Recirculation and improved material selection for high temperature corrosion abatement, Investigating different aspects of corrosion memory ISBN 978-91-7673- 093-5 | © Energiforsk April 2017.
16. M. Montgomery, Y.C Malede, D.Wu, K.V. Dahl *"Danish Experiences in Biomass Corrosion and Recent Areas of Research*" CORROSION, 75:4 (2019) p358-366.
17. D. Wu, K.V. Dahl, J.L Madsen, T.L Christiansen, M. Montgomery, J. Hald: *"Effects of Different Fuel Specifications and Operation Conditions on the Performance of Coated and Uncoated Superheater Tubes in Two Different Biomass-Fired Boilers"* Applied Energy Materials 1, Vol 4, (2018) pp. 1463-1475.
18. D. Lindberg, J. Niemi, M. Engblom, P. Yrjas, T. Laurén, M. Hupa, Fuel Process. Technol. 141 (2016): p. 285-298.
19. M. Montgomery, J. Hald: *Comparison of Steam Oxidation of 18%Cr Steels from Various Power Plants*. Proceedings: EPRI International Conference on Corrosion in Power Plants. Palo Alto, CA : EPRI, 2015. p. 7-22 - 7-32.
20. M. Montgomery, K.V. Dahl, F.B. Grumsen, F.B. Kværndrup, J. Hald *"Nitridation of Grate in a Biomass Fired boiler"*Accepted Materials and Corrosion – in press 2019.

Annex

Add links to relevant documents, publications, home pages etc.
Publications in connection with the biomass corrosion management project.

1. M. Montgomery, L.V. Nielsen, M.B. Petersen: *Utilization of on-line corrosion monitoring in the flue gas cleaning system.* Proceedings International NACE Conference, Dallas TX 2015. Paper 5550. (presented VGB meeting Linz 2014)
2. M. Montgomery, S. Kiamehr, K.V. Dahl: *Danish Experiences in Biomass Corrosion and the Way Forward.* Proceedings: EPRI International Conference on Corrosion in Power Plants. Palo Alto, CA : EPRI, 2015. p. 8-78 - 8-89.
3. M. Montgomery, J. Hald: *Comparison of Steam Oxidation of 18%Cr Steels from Various Power Plants*. Proceedings: EPRI International Conference on Corrosion in Power Plants. Palo Alto, CA : EPRI, 2015. p. 7-22 - 7-32.
4. M. Montgomery, L.V. Nielsen, M.B. Petersen. *Assessment of corrosion in the flue gas cleaning system using on-line monitoring.* VGB PowerTech 10 (2015) pp.77-83.
5. S. Okoro, M. Montgomery, F.J. Frandsen, K. Pantleon: *Alkali chloride induces corrosion of superheater under biomass firing conditions: Improved insights from laboratory scale studies*. Proceedings The Nordic Flame Days 2015.
6. D. Wu, K.V. Dahl, M. Montgomery, K. Pantleon, J. Hald: *Laboratory Investigations of Ni-Al Coatings Exposed to Conditions Simulating Biomass Firing.* Proceedings of the 9th International Symposium on High-Temperature Corrosion and Protection of Materials. 2016
7. S. Okoro, S. Kiamehr, M. Montgomery, F.J. Frandsen, K. Pantleon "*Effect of flue gas composition on deposit induced high temperature corrosion under laboratory conditions mimicking biomass firing. Part I: Exposures in oxidizing and chlorinating atmospheres"* **.** Materials and Corrosion, 68 (2017) p.499-514
8. S. Okoro, S. Kiamehr, M. Montgomery, F.J. Frandsen, K. Pantleon "*Effect of flue gas composition on deposit induced high temperature corrosion under laboratory conditions mimicking biomass firing. Part II: Exposures in SO2 containing atmospheres***"** Materials and Corrosion, 68 (2017) 515-528.
9. M. Montgomery, R.E. Olesen, P. Gensmann: *Corrosion in a flue gas cleaning system of a biomass fired power plant.* Journal of Failure, Analysis and Prevention, 2017 17 p195-204.

10. KME report 714: "*Sulfur Recirculation and improved material selection for high temperature corrosion abatement, Investigating different aspects of corrosion memory"* ISBN 978-91-7673- 093-5 | © Energiforsk April 2017.
11. M. Montgomery, K.V. Dahl, S.A. Jensen, C. Davies: ***"****High Temperature Fireside Corrosion of Esshete 1250 in Coal, Co-firing with Biomass and Biomass Power Plants".* Proceedings Eurocorr 2017, Prague 3-7th September, 2017.
12. M. Montgomery, P. Gensmann "*On-line corrosion measurements undertaken in a flue gas cleaning unit of a biomass fired power plant"* Proceedings Eurocorr 2017, Prague 3-7th September, 2017.
13. S.C. Okoro, F. Nießen, M. Villa, D. Apel, M. Montgomery, F.J. Frandsen, K. Pantleon *"Complementary Methods for the Characterization of Corrosion Products on a Plant-Exposed Superheater Tube"* Metallography, Microstructure and Analysis Vol 6: 1 (2017) pp. 22-35.
14. S.C. Okoro, M. Montgomery, F.J. Frandsen, K. Pantleon *"Influence of preoxidation on high temperature corrosion of a Ni-based alloy under conditions relevant to biomass firing"* Surface and Coatings Technology Vol 319 (2017) pp 76-87.
15. S.C. Okoro, M. Kvisgaard, M. Montgomery, F.J. Frandsen, K. Pantleon "Preoxidation and its effect on reducing high-temperature corrosion of superheater tubes during biomass firing" Surface Engineering 33:6 (2017) pp.428-432.
16. Y.C. Malede, M. Montgomery, K.V. Dahl J. Hald: *Effect of microstructure on KCl corrosion attack of modified AISI 310 steel"* Materials at High Temperatures Vol 35, No 1-3, (2018) pp243-254.
17. D.L. Wu, K.V Dahl, T.L. Christiansen, M. Montgomery, J. Hald *"Microstructural investigations of Ni and Ni_2Al_3 coatings exposed in biomass power plants"* Materials at High Temperatures, Vol 35: 1-3, (2018) pp. 255-266.
18. K.V. Dahl, A. Slomian, T.N. Lomholt, S. Kiamehr, F.B. Grumsen, M. Montgomery, T. Jonsson: *Characterization of pack cemented Ni2Al3 coating exposed to KCl(s) induced corrosion at 600ºC*, Materials at High Temperatures, Vols 35, No.1-3, (2018) pp 267-274.
19. D. Wu, K.V. Dahl, J.L Madsen, T.L Christiansen, M. Montgomery, J. Hald: *"Effects of Different Fuel Specifications and Operation Conditions on the Performance of Coated and Uncoated Superheater Tubes in Two Different Biomass-Fired Boilers"* Applied Energy Materials 1, Vol 4, (2018) pp. 1463-1475.
20. S.C. Okoro, M. Montgomery, F.J. Frandsen, K. Pantleon *"Influence of Preoxidation on High-Temperature Corrosion of a FeCrAl Alloy under Conditions Relevant to Biomass Firing"* Oxidation of Metals 89:1-2 (2018) pp99-122.
21. S. Okoro, M. Montgomery, F.J. Frandsen, K. Pantleon "*Time and temperature effects on alkali chloride induced high temperature corrosion of superheaters during biomass firing".* Energy and Fuels 32 (7) (2018) pp. 7991-7999.
22. D.L. Wu, K.V Dahl, T.L. Christiansen, M. Montgomery, J. Hald *"Corrosion behavior of Ni and nickel aluminide coatings exposed in a biomass fired power plant for two years"* Surface & Coatings Technology 362 (2019) pp 355-365.
23. M. Montgomery, Y.C Malede, D.Wu, K.V. Dahl *"Danish Experiences in Biomass Corrosion and Recent Areas of Research*" CORROSION, 75:4 (2019) p358-366.
24. M. Montgomery, K.V. Dahl, J. Hald *"Corrosion of welds in biomass power plants"* Materials and Corrosion 70 (2019) p585-592.
25. M. Montgomery, K.V. Dahl, F.B. Grumsen, F.B. Kværndrup, J. Hald *"Nitridation of Grate in a Biomass Fired boiler"*Accepted Materials and Corrosion – in press 2019.
26. Y.C. Malede, J.P. Simon, T. Jonsson, , M. Montgomery, K.V. Dahl, J. Hald: "KCl induced corrosion of Ni-based alloys containing 35-45 wt% Cr. Materials and Corrosion 2019 DOI: 10.1002/maco.201810658
27. Y.C. Malede, K.V. Dahl, M. Montgomery, F.B. Grumsen, J. Hald: ***"****Effect of service exposure on KCl corrosion attack of AISI 347H FG steel". Sent to review 2019*